Host shapes microevolution of MDR *Acinetobacter baumannii* during long-term infection

Authors: Léa Bednarczuk[a,b], Alexandre Chassard[a#], Julie Plantade[a#], Xavier Charpentier[a] and Maria-Halima Laaberki[a,b*].

a. CIRI, Centre International de Recherche en Infectiologie, Inserm, U1111, Université Claude Bernard Lyon 1, CNRS, UMR5308, École Normale Supérieure de Lyon, Univ Lyon, 69007, Lyon, France

b. Université de Lyon, VetAgro Sup, 69280 Marcy l'Etoile, France.

#equivalent contributions

*Correspondence to Maria-Halima Laaberki: maria-halima.laaberki@vetagro-sup.fr

Running title: Within-host evolution of *A. baumannii*

Word count: Abstract (226), Importance (121), Text (5695)

Abstract

Acinetobacter baumannii is a nosocomial pathogen associated with various infections, including urinary tract infections (UTIs). *A. baumannii* is known to rapidly become resistant to antibiotic therapy, but much less is known about possible adaptation without antibiotic pressure and thereby host-driven evolution. Through a retrospective study, we investigated within-host microevolution during a subclinical five-year UTI in an animal-patient after withdrawal of colistin treatment. We conducted whole-genome sequencing and phenotypic assays on seventeen ST25 isolates. Eight of which were isolated longitudinally throughout the infection timeline while nine others were obtained subsequently to investigate bacterial diversity. We determined that the infection was monophyletic with variations in genome sizes and nucleotide sequences. Over the course of the infection, *A. baumannii* underwent genome reduction through insertion sequence (IS) recombination, phage excision, or plasmid curing. Despite this global genome reduction, we observed an expansion of IS*17*, initially located on an endogenous plasmid. Gene loss resulted in decreased antibiotic resistance, yet colistin resistance due to a *pmrB* mutation remained stable. All other genetic variations were mainly located in metabolism and biofilm formation genes. Metabolic assays revealed a shift towards as slight decreased metabolic flexibility, presumably adapted to host's urine composition. Moreover, repeated variation affecting biofilm and adhesion genes associated with weak biofilm-forming capacity suggests a genetic drift of repressed genes. This study provides a unique insight into host adaptation of this opportunistic pathogen.

Importance

This study sheds light on the adaptive strategies of *Acinetobacter baumannii* during a five-year UTI in the absence of antibiotic treatment. The observation of both longitudinal strains and synchronic strains highlights the necessity of studying bacterial diversity to understand the evolutive strategies, as relying solely on single-isolate approaches can result in misleading conclusions. By combining genomic and phenotypic analyses, we observed a significant reduction in genome size over the course of the infection, resulting in some loss of metabolism flexibility, adhesion capacities and antibiotic resistance. Altogether, our findings suggest that during infection *A. baumannii* streamlines its genome, discarding unnecessary functions in

53 favor of a more adapted lifestyle to colonize its new environment, possibly reducing its
54 capacity to further cause difficult-to-treat infections.
55
56

57 **Introduction**

58 *Acinetobacter baumannii* is a non-fermentative Gram-negative pathogenic bacterium
59 responsible for nosocomial infections in humans and animals, particularly in intensive
60 care units (1, 2). *A. baumannii* represents a major threat to public health due to the
61 rapid emergence of multidrug-resistant isolates increasingly difficult to eradicate (3).
62 Indeed, few antibiotics remain effective against this pathogen, such as carbapenems,
63 and the carbapenem resistance of clinical isolates may require poorly tolerated
64 antibiotics such as colistin (4). Emergence of carbapenem resistance in *A. baumannii*
65 therefore limits treatment option and led World Health Organization (WHO) to classify
66 carbapenem-resistant strains of *A. baumannii* (CRAB) as a priority for research and
67 development of new drugs (5). This pathogen is also described in animal infections
68 especially in pets with strains belonging to clones common with human medicine with
69 concerning resistance to human restricted antibiotics such as carbapenems (1, 6).

70 This bacterium has no particular tropism, causing mainly pulmonary infections but also
71 capable of skin, blood, bones, urinary tract infections (7). The existence of extra-
72 hospital reservoirs has long been disputed, but recent studies demonstrate that *A.*
73 *baumannii* is an ubiquitous bacterium found both in soils and carried by healthy
74 individuals - humans and animals (8–11). This bacterium is therefore capable of
75 thriving in highly contrasted environments, demonstrating a great capacity for
76 adaptation; antibiotic resistance would be just one facet of its versatility applied to the
77 healthcare context.

78 Several within-host studies of *A. baumannii* infection describe antibiotic resistance
79 emergence in response to treatment due to non-synonymous (NS) single nucleotide
80 polymorphism (SNP) or horizontal gene transfer (12, 13). However, little is known
81 about host adaptation, because brief timeframes of infection limiting observation of
82 bacterial evolution within a host. Additionally, these investigations focused on human
83 infections, typically involving extended antibiotic treatments making difficult to decipher
84 antibiotic from host adaptation. They also involve mostly single-isolate approaches
85 hindering the understanding of within-host diversity. Consequently, there remains a
86 limited understanding of the fate of antibiotic resistance genes and more broadly of
87 gene evolution post-antibiotic exposure and during host colonization. Seminal within-
88 host microevolution studies on *A. baumannii* observed the accumulation of variations
89 in genes involved surface structures such as motility, adhesion, biofilm formation or
90 cell wall and capsule biogenesis, suggesting a consistent selective pressure during

91 antibiotic-treated infections but phenotypic validation are usually missing (14–16).
92 Phenotypically, antibiotic exposure prompts bacteria to adopt a biofilm-like lifestyle,
93 enhancing their resistance (17). These biofilms pose challenges for infection treatment
94 and promote recurrence, notably in urinary tract infections (UTI) (18). Despite the over-
95 representation of pulmonary and bloodstream infections in *A. baumannii* studies, the
96 urinary tract is a major source of *A. baumannii* isolates in human (19). Tissue tropism
97 may result from mobile genetic elements regulation as exemplified by plasmid-driven
98 regulation of chromosomal genes modifying strain adhesion pattern (6, 20, 21).
99 Therefore, *A. baumannii* within-host microevolution may involve crosstalk of mobile
100 genetic element and core genome determinant but clinical evidence is missing.
101 In the following case study, a pet infection emerged from a subcutaneous ureteral
102 bypass placement which was particularly described as a risk factor for development of
103 *A. baumannii* UTI in cats (22). We used whole-genome sequencing and phenotype
104 assays on 17 *A. baumannii* strains isolated from the same cat with UTI over a five-year
105 period without antibiotic treatment. We sought to investigate the fate of antibiotic
106 resistance and explore evolutionary strategies upon infection.
107

108 **Results**

109 **A ST25 monophyletic infection related to human and animal cases**
110 A retrospective study was performed on *A. baumannii* isolates cultured from a single
111 animal-patient (cat) over a 5-year period (2014 to 2019). This patient-animal developed
112 a urinary *A. baumannii* infection following the placement of a urinary invasive medical
113 device. The early isolate was identified as multidrug resistant, including to human-
114 restricted antibiotic carbapenems, but not to colistin. However, two colistin treatments
115 failed to clear the infection. Given the limited antibiotic arsenal authorized in veterinary
116 medicine, , and the absence of invalidating clinical signs, no further antibiotic treatment
117 was attempted. During medical follow-ups, eight strains (referred as longitudinal
118 strains) were sequentially isolated and stored by the hospital laboratory from
119 November 2014 to February 2019 (**FIG S1 & TABLE S1**). In addition, nine strains
120 (referred to as synchronic strains) were subsequently isolated from a single complete
121 urine sample collected on October 2019.

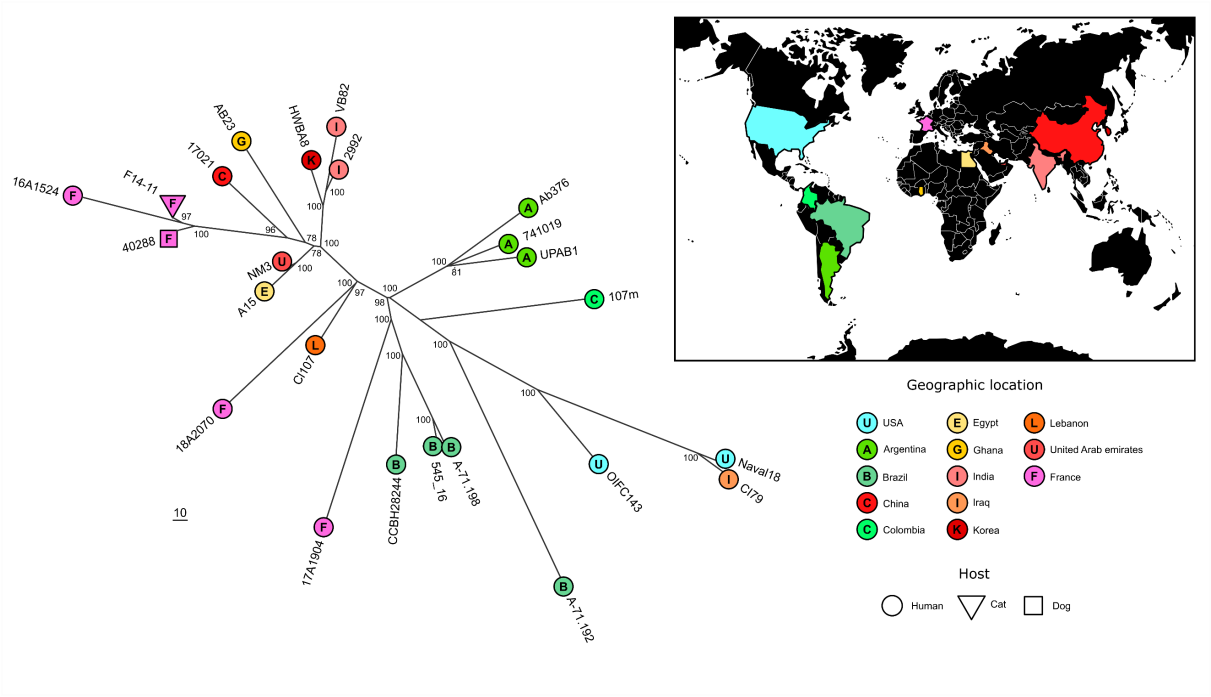

FIG 1. Phylogenetic proximity of F14-11 to other strains isolated from human and animal infections worldwide. (A) Unrooted Maximum Likelihood Phylogeny constructed with Gubbins based on RAxML. Tips are colored according to their geographic site of isolation, annotated with the initial letter of the country, and shaped according to the host. Bootstrap values are indicated at nodes. The scale below shows the length of branches in base substitutions. (B) World map highlighting countries corresponding to the color scheme.

Whole-genome sequencing and hybrid assembly of the seventeen study strains revealed a monophyletic infection with a sequence type (ST) 25 clone, ST associated with UTI in human and animals (6, 20). To identify the closest genomes to F14-11, the earliest isolate, we used the Similar Genome Finder utility of the WhatsGNU tool to query an *A. baumannii* genome database retrieved from the NCBI (5234 genomes, downloaded on February, 17th 2023, 23). Most strains were from human origin as publicly available *A. baumannii* genomes are mostly related to human medicine. The phylogenetic tree constructed from twenty-three ST25 strains reveals an apparent correlation between isolation location and phylogenetic proximity for Eurasian and American distributions. However, both North American strains were probably military imports from overseas explaining their clustering with an Iraqi strain (24) (**FIG 1**). This analysis also indicated a clustering of clones independently of their host implying zoonotic transfer and highlighting the relevance of investigating animal infections for

143 human health (25). The closest human strain, 16A1524, was indeed isolated in France
144 in 2016. Interestingly, the closest strain, 40288, was also isolated in France from a dog
145 UTI in 2015 (26). F14-11 and 40288 exhibit only 31 SNPs across their chromosomes
146 and 1 SNP between their ~145Kb-length plasmids p40288 and pF14-11 (**TABLE S2**).
147 The pF14-11 backbone was also detected in 22 of closest genomes (coverage from
148 65% to 100%, **TABLE S2**). Despite its reduced size, pF14-11 shares 100% identity
149 with plasmids pVB82 (215Kb) and pHWBA8 (195Kb) carried by close eponymous
150 strains (**FIG S2** and **TABLE S2**). This size reduction may explain the inability of pF14-
151 11 to undergo conjugation and reflect its bacterial host's evolution (**FIG S2**).

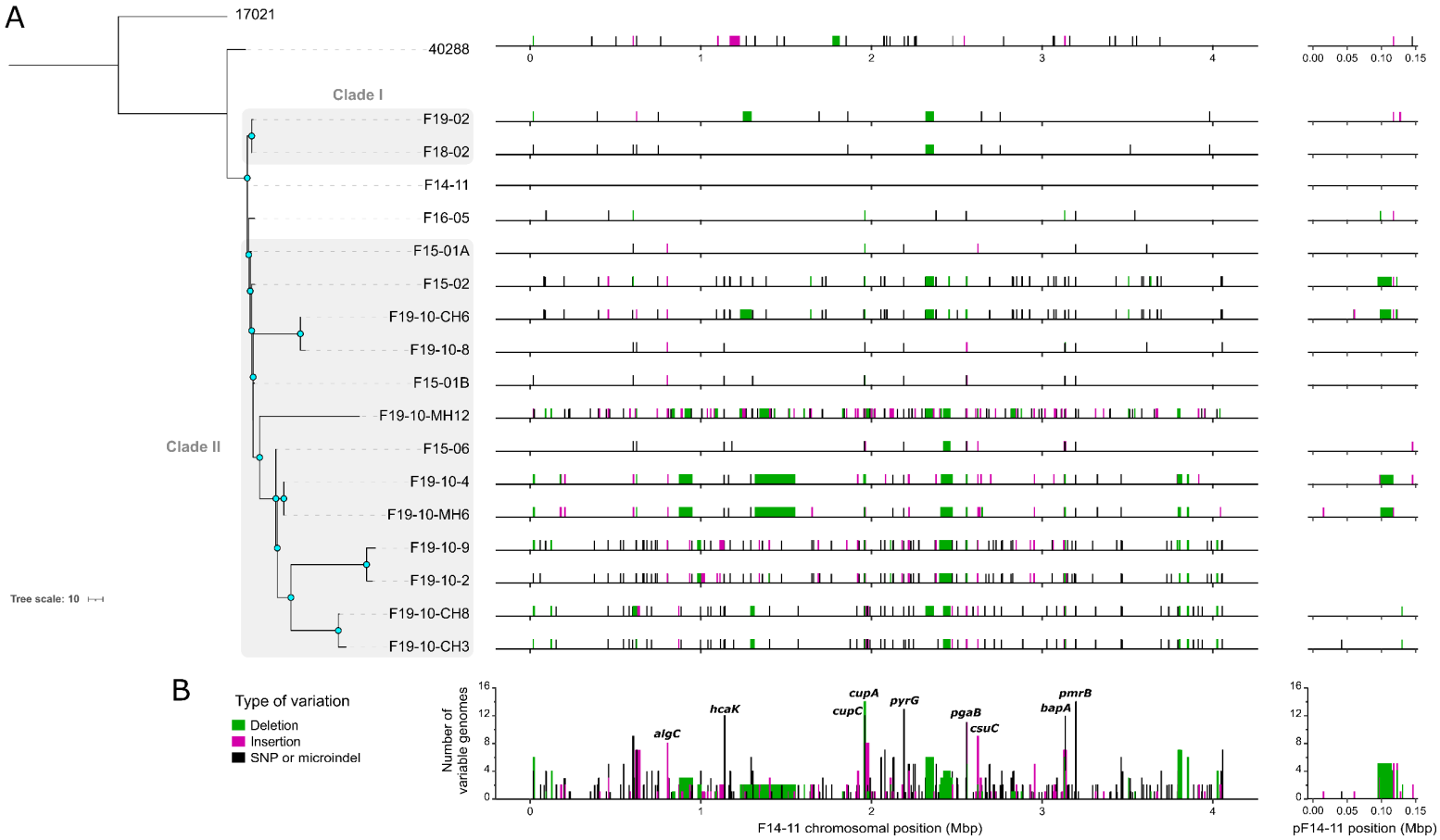

FIG 2. Phylogenic tree of the study strains and 40288 associated with the distribution of the genetic variations. (A) Left: Maximum Likelihood Phylogeny constructed with Gubbins based on RAxML. The tree was rooted with strain 17021. Blue nodes indicate bootstrap values >80. Right: Representation of SNPs and microindels in black, insertions in pink and deletions in green along the genomes in comparison to F14-11 (reference genome). (B) Cumulative distribution of the genetic variations along the F14-11 genome with *y*-axis indicating the number of study strains harboring the genetic variation. The genes most prone to variation are shown.

158 **Genome reduction and insertion sequences proliferation**

159 To further investigate within-host genome evolution, we performed whole-genome
160 comparison of the sixteen study strains to the early one F14-11, set as a reference
161 (**FIG S1** & **TABLE S1** for isolates descriptions). This analysis revealed a low number
162 of SNPs scattered throughout the genome in comparison to F14-11, with a mean of 31
163 SNPs per genome (ranging from 3 SNPs for the closest genomes to 78 SNPs for the
164 most distant one).

165 Phylogenetic analysis suggests an absence of correlation between isolation date and
166 phylogenetic relationships (**FIG 2**). Notably, longitudinal isolates F18-02 and F19-02
167 form an independent clade, referred as clade I, sharing a hypothetical common
168 ancestor with all other strains. In contrast, late synchronic strains isolated in 2019
169 cluster with strains isolated in 2015 implying the coexistence of different lineages
170 during the infection. This monophyletic group, referred as clade II, may have gained
171 competitive advantage over time. In addition, a correlation is observed between the
172 mean chromosome size of strains isolated within the same month and the time elapsed
173 between months of isolation (R^2=0.86, P=6.7×10^{-3}, Spearman test) with a reduction in
174 size during infection (**TABLE S1**). This correlation suggests that a reduced genome
175 may confer a selective advantage in this niche. Genome reduction more frequently
176 operates on mobile genetic elements such as prophages and plasmid. Indeed, most
177 strains show independent excisions of one to three of the four prophages identified in
178 strain F14-11. Close strains F18-02 and F19-02 lost one and two prophages
179 respectively (**FIG 2**, large deletions highlighted in green and **FIG S3A**, prophage
180 regions 2 and 4) probably independently from strains from clade II.

181 A reduction in plasmid size is also observed during the infection. Four of the synchronic
182 isolates lack a 12-18 kb plasmid region corresponding to the BREX phage resistance
183 system while three have lost the plasmid entirely (**FIG 2 & S3B and C**) (27). Moreover,
184 within-host evolution also operates through IS dynamics. Interestingly, the most
185 abundant IS in chromosome originated from the resident plasmid (**FIG S4**). Indeed,
186 IS*17*, an IS*5* family insertion sequence, was absent from the chromosome of the
187 earliest strain, F14-11, but carried by its plasmid pF14-11. While a single instance of
188 IS*17* was found in the chromosomes of strains isolated in 2015, it significantly
189 multiplied in synchronic strains, climaxing with 75 occurrences in strain F19-10-MH12.

190 **Genetic drift of adhesion and biofilm genes**

191 Over 82% of SNPs and microindels of the strains studied are in coding sequences,
192 and 80% of these are non-synonymous, indicating positive selection. Most of these
193 coding sequences are involved in adhesion and biofilm formation that are also affected
194 by insertion and deletion events (**FIG 2**; *cup* (28), *csu* (29), *pga* (30), *bapA* (31), *algC*
195 (32) genes). Strikingly, genes involved in biogenesis of archaic and classical types of
196 chaperone-usher pili involved in adhesion step of biofilm formation (*csu* and *cup*
197 operon respectively) were subjected to IS insertion, deletion and frameshift.
198 Specifically, the *csu* operon is affected by insertions by distinct IS in strains F15-01A
199 (IS*17*) and F15-06 (IS*Aba33*), this latter insertion being conserved in most of
200 synchronic isolates (7 out of 9). Genes of the classical pili Abp1 (formerly Cup), *cupA*
201 and *cupC*, were also affected by large deletions and indel leading to frameshift in most
202 strains of the clade II. Additionally, genes involved in biofilm formation such as *algC*
203 and *pgaABCD* but also *bapA* gene were also disrupted by IS insertion or subjected to
204 deletion events (**FIG 2**).

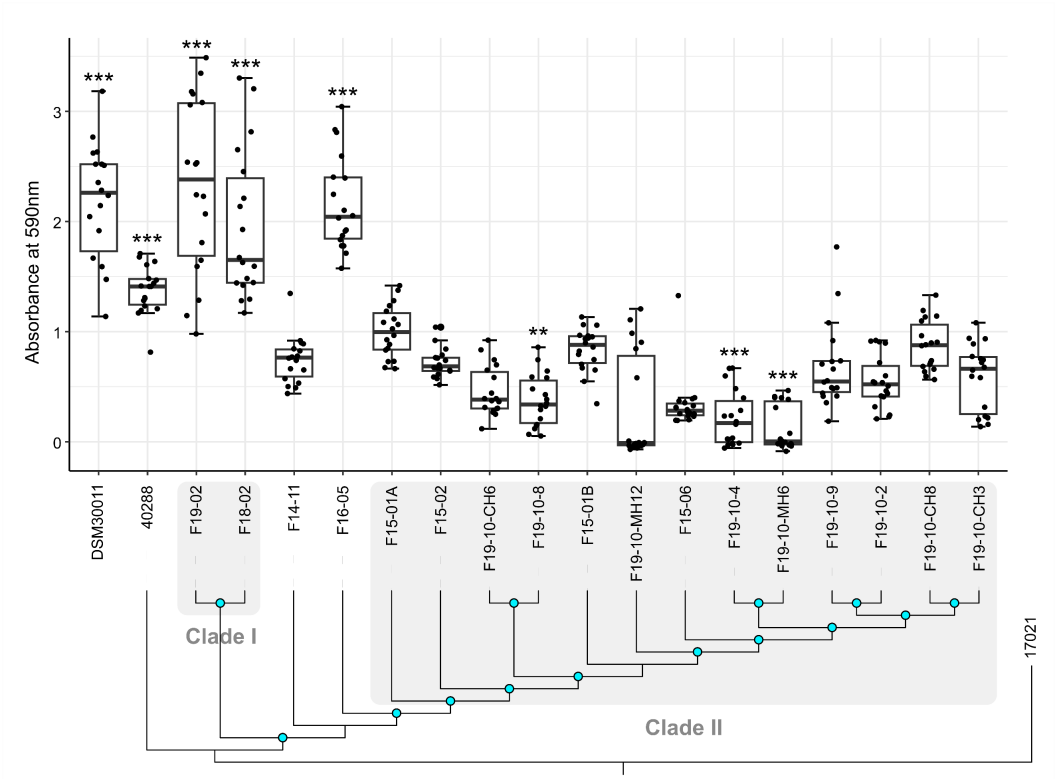

205

206 **FIG 3.** Biofilm formation by the study strains and the dog UTI strain 40288 associated with their
207 phylogenetic relationships. Blue nodes indicate bootstrap values >80. Biofilm formation was
208 assessed by measuring the optical density of crystal violet stained matrix and compared to

209 environmental strain DSM30011. Error bars are generated from 12 replicas from 4 independent
210 experiments. Statistically significant differences with F14-11 (Kruskal-Wallis rank-sum tests with
211 Bonferroni-Holm correction) are highlighted with asterisks: (*) if the p-value < 0.05, (* *) if the p-
212 value ≤ 0.01, and (* * *) if the p-value ≤ 0.001.

213 Hence, adhesion appendages and biofilm components appear dispensable during a
214 prolonged infection. To bring experimental evidence to this hypothesis, biofilm-forming
215 capacities of the study strains were measured and compared with those of the
216 environmental DSM30011 strain described as strong biofilm-producer (**FIG 3**) (33). As
217 observed for human clinical strains, the animal clinical strain F14-11 forms less biofilm
218 than DSM30011 (3-fold; p-value: 0.00143). However, F14-11 carries a plasmid closely
219 related to plasmid pAB5 that downregulates biofilm *pga* and adhesion *cup* genes in
220 strain UPAB1 (20, 21). We therefore tested the hypothesis that pF14-11 may restraint
221 biofilm production. Yet, pF14-11 curing did not increase adhesion, biofilm nor PNAG
222 production (**FIG S5**).
223 Surprisingly, F16-05 isolate is a strong biofilm producer despite a frameshift in the
224 *cupC* gene and a non-synonymous SNP in *pgaB*. However, its adhesion capacity is
225 indeed greatly affected (**FIG S5**). Moreover, in spite of the genome proximity between
226 F14-11, F18-02 and F19-02 these latter two strains produce biofilm amount
227 comparable to DSM30011 (p-value=1) (**FIG 3**). However, none of the SNPs, mainly
228 found in intergenic region, nor the phage deletions of these strains are common
229 between F16-05 and the late isolates and could account for this phenotype. The strong
230 biofilm production by these three strains, indicate that biofilm production is repressed
231 in F14-11 strain by a chromosomally encoded factor. In contrast, strains from the clade
232 II exhibit comparable or reduced biofilm production in comparison to F14-11. However,
233 considering the numerous adverse variations in their adhesion and biofilm genes, a
234 more drastic reduction in biofilm formation was expected. In addition, F14-11, despite
235 identical biofilm and adhesion genes (*cup*, *csu*, *pga*, *algC* genes), produces less biofilm
236 than dog UTI strain 40288 (p-value: 1.3e-05). We tested if the residual biofilm capacity
237 of F14-11 involved type IV pili or *prp* type I pili but fail to identify its adhesion
238 mechanism (**FIG S5**).
239 Altogether, these results indicate that the F14-11 strain isolated at an early stage of
240 infection exhibits low biofilm production, probably due to repression of biofilm genes
241 by a chromosomally encoded factor. These repressed genes were probably subjected

242 to genetic drift. However, our results indicate that weak and strong biofilm-producing
243 populations probably coexist but sampling method may favor isolation of planktonic
244 cells.

245 **Colistin resistance fixation but overall resistance loss**

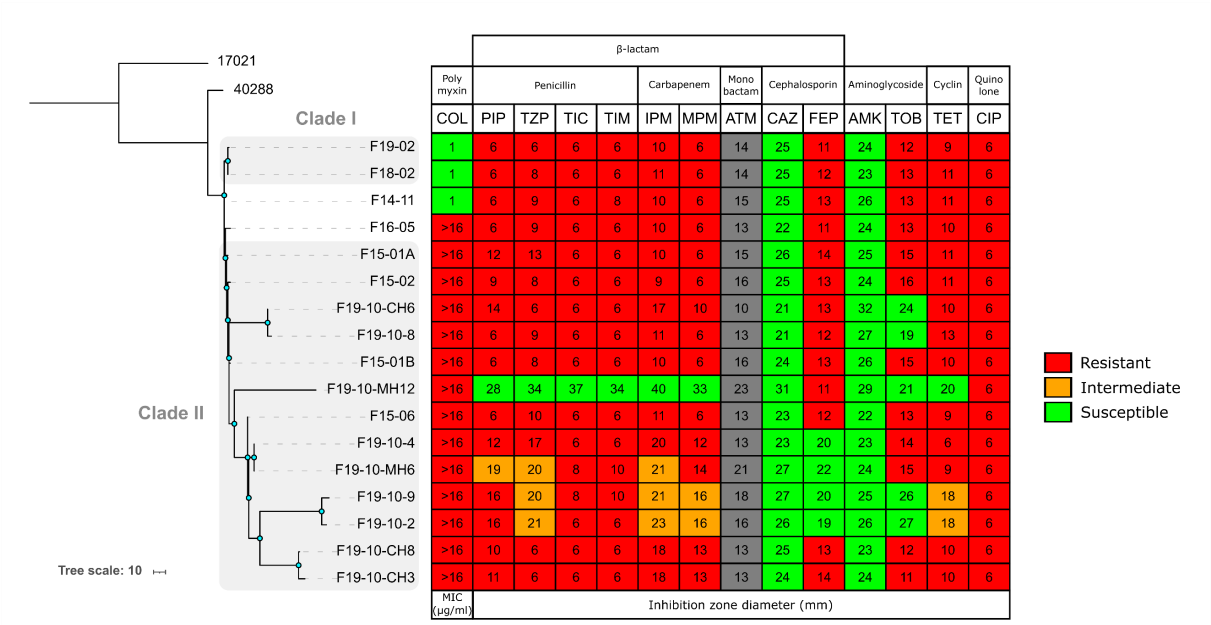

246

247 **FIG 4**. Heatmap of antibiotic susceptibility of the study strains associated with their phylogenetic
248 relationships. Blue nodes indicate bootstrap values >80.. Abbreviations. AMK: Amikacin, GEN:
249 Gentamicin, TOB: Tobramycin, CIP: Ciprofloxacin, PIP: Piperacillin, TZP: Piperacillin +
250 tazobactam, TIC: Ticarcillin, TIM: TIC + clavulanic acid, CAZ: Ceftazidime, FEP: Cefepime, IMP:
251 Imipenem, MEM: Meropenem, ATM: Aztreonam, TET: Tetracycline, COL: colistin. Antibiotic
252 susceptibilities were either measured using minimal inhibition concentration (MIC) or by the disk
253 diffusion methods. The antibiotics tested are listed on the x-axis and the study strains on the y-
254 axis.

255 The first isolate F14-11 is resistant to penicillins, cephalosporines (but ceftazidime),
256 fluoroquinolones, aminoglycosides (but amikacin) and carbapenems. Following colistin
257 treatments, colistin resistance developed in 2015 isolates (**FIG 4**). Colistin resistance
258 was mainly maintained after cessation of treatment with the exception of two sensitive
259 isolates (F18-02 and F19-02). Colistin resistant isolates share a PmrB(P170T)
260 substitution. We ensured that PmrB(P170T) transfer to F14-11 resulted in colistin
261 resistance (MIC>16µg/mL). Contrarily to PmrB(P170L) associated to a growth defect
262 in laboratory define medium (34), F14-11 derivatives PmrB(P170T) and parental F14-
263 11 have comparable growth rate (**FIG S6**). Interestingly, isolation of colistin-sensitive

264 strains with wild type *pmrB* sequence suggests coexistence of both resistant and
265 sensitive strains (**FIG 4** ; F18-02 and F19-02).
266 In contrast to colistin resistance, several antibiotic resistances were lost in the clade II
267 in comparison to F14-11. Most susceptibilities emerged due to plasmid loss. Early
268 isolate plasmid pF14-11 harbors genes conferring resistance to tetracycline (*tetA(B)*),
269 aminoglycosides (*strA/strB, aac(3)-IIa, aac(6')-Ian*) and sulfonamides (*sul2*) frequently
270 associated with this family of plasmid (25). Plasmid loss expectedly results in
271 susceptibility to tetracycline and tobramycin as observed for strains F19-10-MH12,
272 F19-10-2, and F19-10-9 (**FIG 4**). However, plasmid loss alone may not explain
273 recovered susceptibility to antibiotics as two tobramycin-sensitive strains still carry a
274 plasmid (**FIG 2 & 4**; F19-10-CH6 and F19-10-8). Their intact resistance gene
275 sequences led us to hypothesize that plasmid-specific deletion events encompassing
276 a putative DNA primase encoding gene may lower plasmid copy number and maybe
277 decrease associated resistance to tobramycin.
278 Chromosomal resistance carried by mobile genetic elements were also subjected to
279 curing. F14-11 strain carries two copies of Tn*2006* carrying bla_{OXA-23} gene accounting
280 for its carbapenem resistance. Closely related strain 40288 also bears two Tn*2006*
281 copies located either in an AbaR4 resistance island inserted in the *comM* gene or
282 interrupting the *vgrG* gene (26) . Compared to 40288, F14-11 present a recombination
283 event between Tn*2006* copies leading to a split AbaR4. Further deletions of one or two
284 Tn*2006* in several strains may explain increased susceptibility to carbapenems (**FIG 4**
285 ; respectively in F19-10-4, F19-10-CH3, F19-10-CH8 F19-10-MH6 and F19-10-MH12).
286 Additionally, resistance decreases without antibiotic gene loss may be related to
287 compromised growth in laboratory medium associated with large chromosomal
288 deletion events (**FIG 4 & S7**; F19-10-2, F19-10-9 and F19-10-MH6). Taken together,
289 these results indicate an overall decline in antibiotic resistance mediated by curing of
290 mobile genetic elements. They also suggest coexistence of strains with varying
291 resistance levels within a population hence illustrating within host heteroresistance
292 even in the absence of antibiotic pressure.

293 **Adaptation to urine composition**

294 Bacterial metabolism versatility is a crucial factor for successful colonization of a new
295 environment. Similarly to humans, cat's urine composition is highly variable and
296 complex with thousands of unique compounds (35, 36). The variations occur both

among different individuals and within the same individual over time, under the influence of environmental factors, particularly the type of diet (35). Interestingly, genetic variations in study strains mainly occur in metabolic genes (**FIG S8**).

For instance, most strains (13/17) have a substitution in *pyrG* gene encoding the putative PyrG enzyme catalyzing amination of UTP to CTP thereby regulating intracellular CTP levels (**FIG 2**) (37). The non-synonymous substitution (H193R) being in the vicinity of the conserved putative UTP binding site we hypothesized that it increases the enzyme affinity for its substrate. To further explore the metabolism capacities of study strains, we utilized Biolog metabolic phenotypic microarray.

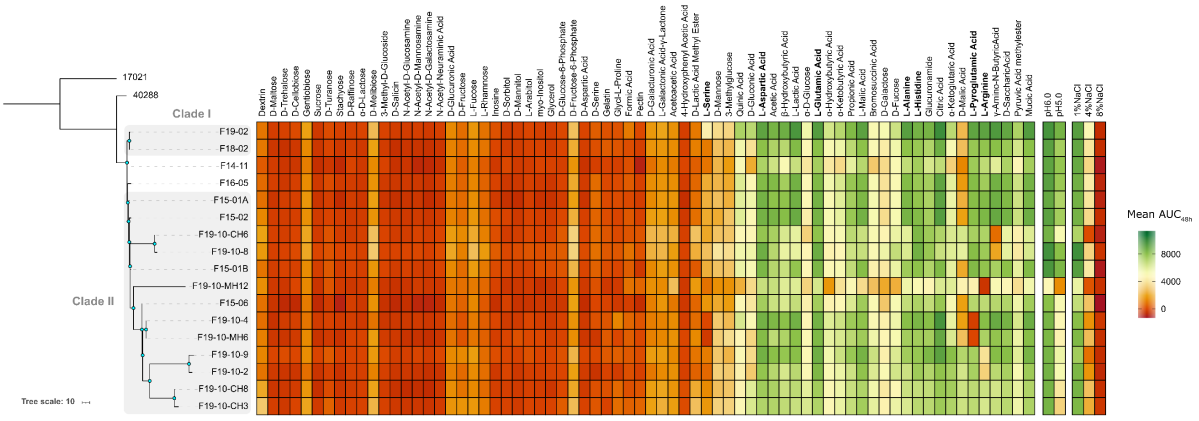

FIG 5. Heatmap of AUC_{48h} for growth either in 70 different nutrient sources, or two pH and three salinity conditions associated with strains phylogenetic relationships. Blue nodes indicate bootstrap values >80. Amino acids are highlighted in bold. The AUC_{48h} parameter was extracted from kinetic data over 48 h in Biolog Gen III MicroPlate. The highest and lowest AUC_{48h} are indicated by green and red colors, respectively. The different compounds and conditions tested are listed on the x-axis and the study strains on the y-axis. Mean data of two independent experiments are shown.

Strains demonstrate an overall poor ability to grow in carbohydrates but were able to utilize most amino acids as sole nutrient source (**FIG 5**). This shared metabolic profile is advantageous in the context of urinary infection as urine usually lacks carbohydrates whereas amino acids and small peptides are abundant (35, 36). The metabolic profiles of the different strains were mostly similar, with the exception of F19-10-MH12 strain whose metabolic capacities may have been profoundly affected by numerous IS*17* insertions (**FIG 5 & S4**). For all nutrient sources tested, metabolic capacities were only marginally altered by allelic variation, transposition, or large deletion. Indeed, a P51H substitution likely abrogated GABA permease function resulting in a growth defect in

322 GABA in strains F19-10-8 and F19-10-CH6. IS*Aba53* insertion upstream an amino
323 acid transporter and downstream an arginine *N*-succinyltransferase may account for
324 slower growth on L-arginine, with ~2-fold lower area under the curve over 48 hours
325 (AUC_{48h}) of strains F19-10-2 and F19-10-9 compared to F14-11. Moreover, a 37Kb
326 deletion occurring in F15-06 likely mediated by recombination between two IS*Aba34*
327 insertion sequences is conserved in most strains of the clade II (but F19-10-8). The
328 deleted region encompasses 27 genes including 19 metabolism genes whereas only
329 40.8% of F14-11 genes are of this category (1533/3758). Besides, large deletion of
330 232.7Kb encompassing 192 metabolism genes found in F19-10-4 and F19-10-MH6
331 strains may impair growth on L-pyroglutamic acid. These large deletions indicate a
332 dispensability of associated metabolic functions for growth in urine.
333 Surprisingly, seven strains exhibit a more efficient growth with D-malic acid with up to
334 ~5-fold higher AUC_{48h} for F19-10-2, F19-10-9, F19-10-CH3, F19-10-CH6 and F19-10-
335 CH8 compared to F14-11. This gain of function for utilization of an artificial amino-acid
336 may reflect an increase efficiency of enzymes from the tricarboxylic acid (TCA) cycle
337 and the requirement of this metabolism pathway for growth in the urinary tract as
338 observed for Uropathogenic *E. coli* (38). An alternative explanation would be an
339 increased metabolization of D-malic acid that is a food preservative authorized in
340 animal feed (39). This unexpected gain in function, may therefore reflect adaptation to
341 the host's urine composition. An adaptation to this specific environment shaped by host
342 diet may also explain the repeated gene evolution found in 14 strains out of 17 for
343 aminobenzoate utilization (*hca* operon, **FIG 2**). Strains presented either a non-
344 synonymous substitution (G269V) in the putative membrane transporter HcaK, and a
345 stop codon mutation in the gene encoding its putative repressor HcaR, indicating a
346 possible increase in aminobenzoate utilization. This family of compounds can be found
347 in human and animal food, sometime used as food preservative and are excreted in
348 urine (40). Lastly, in comparison to F14-11, most strains of the clade II exhibited a
349 significant growth deficiency under low pH conditions as well as under high
350 concentrations of NaCl (4% NaCl). A synonymous and a non-synonymous
351 substitutions in the *bauA* gene may reflect a selective pressure for pH adaptation (F19-
352 10-2 and F19-10-9; F19-10-CH6 and F19-10-8) (41). Indeed, clinical urine tests carried
353 out at the beginning of the infection revealed a neutral pH (7.48). Besides, food diet for
354 cats with urinary disease usually promotes urine pH between 6 to 6.5 and leads to

355 NaCl concentration around 0.5% (42). Therefore, the evolved profile may once again
356 result from adaptation to host's urine specific composition.
357
358
359
360 .

361 **Discussion**

362 High versality of certain clones of *A. baumannii* may explain their ability to colonize
363 various host and dominate the global epidemiology of this pathogen. In this study, we
364 examined within-host genomic evolution during prolonged urinary infection of a ST25
365 strain in an animal host. The genetic proximity between this animal strain and human
366 strains strongly favors the hypothesis of a zoonotic transmission, with a potential
367 transmission from a human to animal hosts (a cat for F14-11 strain and a dog for 40288
368 strain). A relatedness between human and animal isolates of the ST25 lineage was
369 also suggested by a recent study (25). Remarkably, most animal ST25 strains
370 analyzed in this latter study were isolated from urinary infection in greater extent than
371 for human strains suggesting a host-specific tropism. Following transmission, the strain
372 described in our study have further evolved by mutations, insertions and deletions
373 presumably mediated by intragenomic rearrangements. These latter two genetic
374 variations involve IS dynamics known to promote evolution *in vitro* (43, 44). We
375 described that the only plasmid copy of IS*17* was subsequently detected in
376 chromosomes of evolved strains collected during the infection. This result brings
377 additional evidence of IS dynamics shaping bacterial evolution to adapt to a new
378 environment, as recently described for IS*1* in clinical Enterobacteriacea (45).

379 Genetic variations are mainly observed in genes associated with biofilm formation and
380 metabolism. Strikingly, we found that two of three type I *pili* structures encoded by
381 these ST25 isolates were profoundly affected by mutations (*csu* and *cup* genes).
382 Interestingly, several studies described recurrent downregulation or mutation affecting
383 of the *csu* operon following infection by human clinical isolates (15, 34, 46). Besides
384 type I *pili*, other biofilm formation genes present genetic variations such as *algC* and
385 *pga* operon. The *cup* and *pga* genes were also described as downregulated by large
386 conjugative plasmid of a urinary strain involving plasmid-encoded transcriptional
387 regulators that directly or indirectly repressed their expression (20). For the present
388 study urinary strain, curing the related large plasmid or deletion of transcriptional
389 regulators did not modify adhesion pattern suggesting that a strong repression of these
390 genes may also involve chromosomal determinants. Therefore, plasmid-mediated
391 regulation may be indirect involving interplay with chromosomal regulatory pathways
392 of adhesion and biofilm genes. Study strains may have adapted their chromosomal
393 regulatory pathway to alleviate plasmid regulation. Repression of biofilm and adhesion

394 gene expression indicates a dispensability for infection and may have subsequently
395 led to their evolution by genetic drift. This hypothesis is strongly sustained by the
396 recurrent and varying types of gene inactivation observed in those loci. This evolution
397 implies that evolved strains would be impaired in further colonization and infection.
398 Convergent evolution towards loss of function in several of the study strains may even
399 suggest a purifying selection against those traits. Indeed, adhesive structures such as
400 *pili* are highly immunogenic and are even being exploited for vaccine development
401 (47). Loss of these appendages would result in an escape from the host immune
402 system. A heterogenous bacterial population with fluctuating phenotypes may reflect
403 an evolutionary adjustment in the balance between adherence and camouflage.
404 Furthermore, our data suggest a coexistence of strong and poor biofilm-producers
405 rather than a homogenous population. This coexistence was also described in other
406 urinary pathogen during a long-term human urinary infection with *Klebsiella*
407 *pneumoniae* (48). These observations may indicate heterogeneous occupation of the
408 urinary tract with spatially distinct niches. Alternatively, strong and poor biofilm-
409 producers could collaborate, with sufficient extracellular matrix to allow poor biofilm-
410 producer strains to embed themselves in the biofilm. Our study also present
411 divergences with previous studies on human infections. Indeed, we observed only few
412 mutations in translational machinery genes or in genes related to replication,
413 recombination, and repair (16, 46). However, these evolutions may have been shaped
414 by alternative antibiotic treatments performed on human patients. Moreover, contrarily
415 to previous report, colistin resistance was maintained in the study strains. Snitkin *et al.*
416 isolated colistin-sensitive strains from human patients after removal of this antibiotic
417 (46). However, this study used a single-isolate approach randomly isolated that may
418 not reflect the overall population. Alternatively, the PmrB(P170T) may represent a low-
419 cost mutation or even be beneficial in the context of urine infection. Indeed, recent
420 findings on PmrAB indicate that this two-component system responds to low pH (5.8)
421 and metal ions (Fe^{2+}, Zn^{2+} and Al^{3+}) (49). Therefore, PmrB(P170T) mutation could have
422 been maintained to mitigate a urine component toxicity. The metabolic genes have
423 undergone the strongest evolution within the host during this long-term infection. This
424 trend is also observed in longitudinal within-host studies conducted on other bacterial
425 species indicating common survival strategies (50–53). However, strains display an
426 unexpected stable metabolism profile. This observation may reflect our technical
427 limitation as only 70 nutrient sources were tested. Nevertheless, the reduced genomes

428 may be sufficient to efficiently grow on nutrients available in their host environment,
429 such as amino acids, and even to adapt to this specific medium with as near neutral
430 pH, low sodium and chloride, and even presence of diet-associated compound (D-
431 malic acid metabolism, utilization of aminobenzoate). This latter observation brings
432 new perspectives to the management of patients suffering from *A. baumannii* infection,
433 and the potential role of host diet in patient care.
434 Our results also unveiled a hidden phenotypic and genetic diversity within a clinical
435 sample. Rather than to restrict conclusion to a single isolate with defined
436 characteristics, the advent of new sequencing technology such as single-cell
437 sequencing should enable a comprehensive understanding of pathogen genomic
438 dynamics during infection (54).
439

440 **Materials and methods**

441 **Strains**
442 *A. baumannii* strains identified in the Laboratoire Vétérinaire Départemental du Rhône,
443 France (LVD69) were stored in an archive since 2014. Nine strains originated from
444 distinct urine samples collected between 2014 and 2019 and referred to as the
445 longitudinal strains, while all others were derived from a single urine sample collected
446 later in October 2019, referred to as the synchronic isolates. Samples were obtained
447 not for the purpose of this study or research, but rather for diagnostic purposes. The
448 longitudinal strains were initially isolated on a blood agar plate and the synchronic
449 strains were isolated using three different media: LB (Lysogeny Broth, Sigma) agar,
450 Mueller-Hinton agar (Sigma) and CHROMagar *Acinetobacter* (CHROMagar). All the
451 strains used in this study are listed in Supplemental **Table S1**.

452 **Metabolic assays**
453 Metabolic assays were conducted using Biolog Gen III Microplates (Hayward, CA)
454 following the manufacturer's instructions. In brief, the strains were streaked on LB-agar
455 and incubated over night at 30°C. For each strain, a single colony was resuspended
456 in inoculating fluid A (IFA, Biolog) using a cotton-tipped Inoculatorz swab (Biolog) to
457 reach a cell density of 90-98%. Each well of the Gen III MicroPlate, containing either a
458 specific carbon source or a chemical sensitivity testing agent, were filled with 100 µL

459 of the bacterial suspensions and incubated at 33°C for 48 hours in the OmniLog
460 incubator/reader measuring the reduction of tetrazolium redox dye (forming a purple
461 color) due to bacterial growth.

462 **Genome sequencing and annotation**

463 Bacteria were grown in liquid LB medium and DNA was purified using Wizard genomic
464 DNA kit (Promega). DNA quantifications were performed using Qubit™ dsDNA HS
465 Assay Kit (Thermo Fisher Scientific). For each isolate, Oxford Nanopore and Illumina
466 DNA sequencings were both performed. Nanopore sequencing were performed using
467 MinIon flow cells [FLO-MIN106] using the SQK-RBK004 barcoding kit. Illumina
468 sequencing was performed on Illumina HiSeq 2000 with paired 150-base sequence
469 reads (Novogene). Each read set was assembled individually using Unicycler (version
470 0.4.9, 41) and annotated using Prokka (version 1.14.5, 42) on the Galaxy pipeline
471 using as reference AB5075-UW protein sequences (GeneBank accession number:
472 CP008706.1). For analysis purposes, plasmid pF14-11 was annotated using pA297-3
473 sequence (GeneBank accession number: KU744946) except for the *tet*R genes that
474 were named after pAB04 (Genebank accession number: CP012007, 19, 49–52).
475 Putative prophages were predicted using PHASTER (59). Putative resistance genes
476 were detected using Resfinder (version 4.5.0, 54) and insertion sequences using
477 ISfinder (61). All genomes are available at NCBI under BioProject PRJNA1100485.

478 **Construction of bacterial strains**

479 All the oligonucleotides used in this study for genetic modification are listed in
480 supplementary **TABLE S3**. Gene disruptions were performed using a scarless genome
481 editing strategy described previously (26). For plasmid curing of strain F14-11, its
482 Δ*higA-higB::sacB-aac4* derivative was grown overnight in LB (2mL) at 37°C, the next
483 day, 100µL were spread on M63 with 10% sucrose for 24h growth at 37°C then purified
484 on the same medium. About 150 sucrose-resistant CFUs were then patched on LB
485 agar, LB Tetracycline 30µg/mL, LB Apramycin 30µg/mL. Tetracycline and apramycin
486 resistant clones were screened by PCR and plasmid extraction for plasmid loss.

487 **Phylogenetic analysis of the study strains**

488 All chromosomes were aligned to the F14-11 chromosome, set as a reference, using
489 the Gubbins script generate_ska_alignment.py, which creates an alignment using split

490 k-mer analysis version 2 (SKA2, version 0.3.7, 58). The strain 17021 was additionally
491 included to root the tree. This strain is a suitable root as it lies outside the other study
492 strains while still being phylogenetically close. Maximum likelihood tree reconstruction
493 was performed with Gubbins (version 3.2.1, 57) relying on RAxML using the
494 GTRGAMMA model (version 8.2.12, 56) for constructing the phylogeny in each
495 iteration to mitigate the bias of horizontal sequence transfer mechanisms. Statistical
496 support for internal branches of the tree was evaluated by bootstrapping with 10,000
497 iterations. Tree visualization was conducted using iTOL (version 6.9, 57).

498 **Phylogenetic analysis with other closely related ST25**

499 Given the close genetic relationships among the study strains, only the first isolated
500 one, F14-11, was used for the selection of closely related strains from other studies.
501 The topgenome (-t) feature of WhatsGNU was used to identify the ten closest strains
502 from a database comprising 4,325 genomes of *A. baumannii* available on GenBank.
503 The database was constructed by downloading all publicly accessible genomes of *A.*
504 *baumannii* from NCBI in February 2023 (Genome database, search criteria: assembly
505 level = {Chromosome, Complete, Contig}, exclude partial, exclude anomalous).
506 To expand the diversity of the strains set, the top genomes of strains from the top 10
507 closest strains of F14-11 as well as four additional ST25 strains (OIFC143, CI79,
508 Naval18 and 107m) were also included. To prevent erroneous conclusions regarding
509 geographic proximity, only one strain per study was included. Incomplete sequenced
510 genomes were excluded. All the genomes were mapped to the F14-11 chromosome
511 set as a reference using the Gubbins script generate_ska_alignment.py, which creates
512 an alignment using SKA2 (version 0.3.7, 58). The output was then analyzed by the
513 Gubbins algorithm relying on RAxML using the GTRGAMMA model (version 8.2.12,
514 58) for constructing the phylogeny in each iteration to generate an unbiased phylogeny,
515 excluding sequences predicted to be horizontally acquired. The reproducibility of the
516 node positions in the tree topology was assessed using bootstrap analysis with 10^4
517 replicates. No root was assigned because strains known to be outgroups were
518 genetically too distant. Including such distant outgroups would result in insufficient
519 sequence alignment and therefore insufficient information for accurate phylogenetic
520 analysis. Finally, the tree was visualized, incorporating host and isolation location data,
521 using ggtree (version 3.12.0, 58).

522 **Variant detection analysis**

523 Primary Illumina sequence reads (fastq) of monophyletic isolates were aligned to the
524 earliest (F14-11), using the tool snippy (Galaxy version 4.6.0, 59). The primary Illumina
525 reads of the F14-11 strain were also subjected to the analysis as control and returned
526 no SNPs. Deletions, insertions and rearrangements were identified using the software
527 package MAUVE (version 2.4.0, 60). The list of the identified genetic variations is
528 provided in **TABLE S3**.

529 **Antibiotic susceptibilities testing**

530 Susceptibility of the strains to a panel of antibiotics was evaluated by disc diffusion on
531 Mueller-Hinton agar (Biorad, France) following the CA-SFM 2013 recommendations
532 (https://resapath.anses.fr/resapath_uploadfiles/files/Documents/2013_CASFM.pdf).
533 Inhibition values were interpreted according to CA-SFM 2013 breakpoints for all
534 antibiotics but aztreonam, for which *Pseudomonas* spp. breakpoints are given. The
535 strain *Pseudomonas aeruginosa* CIP 7110 was used as control for all the antibiotic
536 susceptibility testing. MIC experiments were also conducted to evaluate susceptibility
537 to colistin and piperacillin according to EUCAST guidelines (68).

538 **Biofilm formation assay**

539 Biofilm-forming capacities of the isolates were evaluated using the crystal violet
540 staining method, with slight modifications to the protocol previously described (69).
541 Briefly, exponential phase cells were inoculated into 96-well polystyrene plates in
542 200µL of BM2 minimal medium (33) supplemented with 10mM potassium glutamate
543 (BM2G) at starting OD_{600} of 0.1 and incubated at 37°C in the absence of light for 48
544 hours, without shaking. The medium was replaced with fresh BM2G medium after 24
545 hours of incubation. After 48 hours, the cells in suspension were removed and the
546 adherent cells were fixed with 3.7% formaldehyde for 10 minutes. The wells were then
547 washed twice with distilled water and 200µL of 0.1% crystal violet was added to each
548 well, incubated for 10 minutes, and washed three times with distilled water. To
549 solubilize the crystal violet, 200µL of 95% ethanol was added and the absorbance was
550 measured at 590nm with Infinite M200 PRO (TECAN) and Magellan 7.1 SP1 (TECAN).
551

552 **Acknowledgments**

We thank Agnese Lupo and Marisa Haenni (Anses Lyon, Unité Antibiorésistance et Virulence Bactériennes, France) for performing antimicrobial susceptibility tests and Maxime Bruto (Anses Lyon, UMR Mycoplasmes, France), Lucie Etienne and Carine Rey (CIRI, France) for fruitful discussions and comments on phylogenetic analysis. This work was supported by the LABEX ECOFECT (ANR-11-LABX-0048) of Université de Lyon, within the program "Investissements d'Avenir" (ANR-11-IDEX-0007) operated by the French National Research Agency (ANR) and by the RESPOND program of the Université de Lyon (UDL). LB was supported by VetAgro Sup (PhD funding). AC was supported by Fondation pour la Recherche Médicale (FRM) (PhD funding).

564 **Supplementary materials**

565 **Supplementary methods**

566 **Conjugation assays**

567 Rifampicin-resistant derivatives *A. nosocomialis* M2 and *A. baumannii* strains AB5075 and A118
568 (26) were used as recipient strains for plasmid donor strains (ATCC17978 carrying pAB3 or F14-
569 11 carrying pF14-11). Overnight cultures in liquid LB were grown at 37°C for recipient and donor
570 strains were mixed equally and 50 µl aliquots were spotted on LB agar medium. Each culture was
571 also mixed with the same volume of LB medium for control spots. After 24h incubation at 37°C,
572 bacteria were resuspended in LB medium and plated on selective medium (rifampicin 100 µg/ml in
573 combination with tetracycline 30 µg/ml for conjugation of pF14-11, or with sulfamethoxazole 30
574 µg/ml and trimethoprim 5 µg/ml for conjugation of pAB3), as well as on LB medium supplemented
575 with rifampicin (100 µg/ml) for numbering of recipient bacteria. Conjugation frequencies were
576 calculated as the ratio of the number of conjugants to the total number of bacteria.

577 **Congo red binding quantification**
578 Congo red binding capacities of strains were quantified using the protocol previously described
579 (21). Briefly, two drops of overnight cultures of each strain were incubated on YESCA agar media
580 supplemented with 50 µg/ml Congo red and Brilliant Blue G 1µg/ml at 37°C in the absence of light
581 for 48 hours, without shaking. The cells were then recovered and washed twice with 50 mM
582 potassium phosphate buffer. The cells were resuspended in 1 mL of this buffer and the OD_{600} was
583 adjusted to 1. A 100 µL aliquot of each sample was transferred to a 96-well polystyrene plates, and
584 the fluorescence of Congo red was measured using a microplate reader with an excitation
585 wavelength of 485 nm and an emission wavelength of 612 nm. Buffer was used as the blank.

586 **Adhesion assays**
587 The *sf-gfp* gene was integrated into the *attTn7* site of all strains of interest. Exponential phase cells
588 of the resulting fluorescent strains were inoculated into uncoated 24-well Ibidi microscopy plate in
589 500µl of LB medium at starting OD_{600} of 0.1 and incubated at 37°C in the absence of light for 1
590 hour, without shaking. After incubation, the cells in suspension were removed and the adherent
591 cells were fixed with Antigenfix for 15 minutes. The wells were then washed twice with distilled
592 water. Four images per wells were collected with a Yokogawa CQ1 using a 40× objective.
593 Fluorescent bacteria on these images were counted using the Yokogawa data analysis software.
594
595
596
597

598 **Supplementary figures and tables**

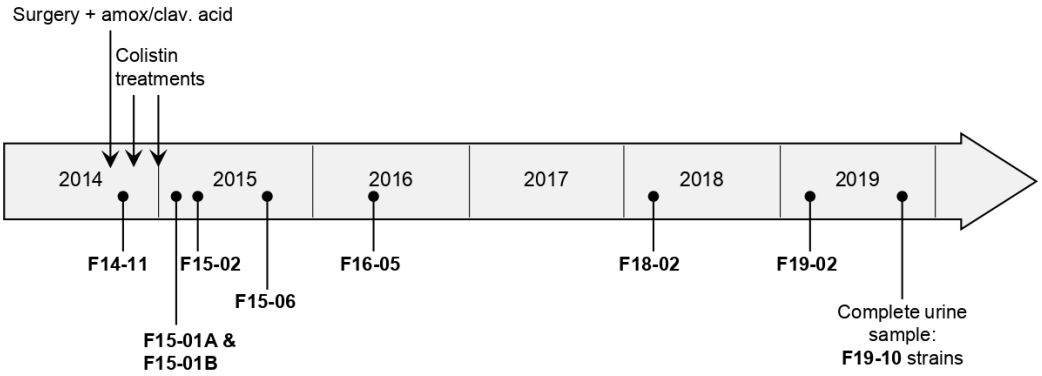

599

600 **FIG S1**. Chronological representation of antibiotic treatments and bacterial isolation. Vertical
601 arrows indicate a postoperative antibiotic prophylaxis with amoxicillin-clavulanic acid (amox/clav.)
602 and two colistin treatments. Isolates are named after the year and month of isolation.

603 **TABLE S1**. Isolation medium, chromosome and plasmid sizes and number of SNP in comparison
604 to F14-11 of the study strains.

	Strain	Date of isolation	Isolation medium	Chromosome size	Plasmid size	Number of SNPs
Longitudinal strains	F14-11	Nov-2014	blood agar	4,061,790	145,509	0
	F15-01A	Jan-2015	blood agar	4,063,881	145,508	3
	F15-01B	Jan-2015	blood agar	4,063,898	145,508	5
	F15-02	Feb-2015	blood agar	4,062,013	145,508	5
	F15-06	June-2015	blood agar	4,029,029	145,709	19
	F16-05	May-2016	blood agar	4,060,980	145,522	5
	F18-02	Feb-2018	blood agar	4,018,678	145,508	3
	F19-02	Feb-2019	blood agar	3,974,547	146,537	4
Synchronic strains	F19-10-2	Oct-2019	LB-agar	4,015,145	-	76
	F19-10-CH3	Oct-2019	CHROMagar	4,027,485	145,482	64
	F19-10-4	Oct-2019	LB-agar	3,687,116	132,823	22
	F19-10-CH6	Oct-2019	CHROMagar	4,017,757	127,468	34
	F19-10-MH6	Oct-2019	Mueller-Hinton-agar	3,692,337	131,775	22
	F19-10-8	Oct-2019	LB	3,971,674	132,530	36
	F19-10-CH8	Oct-2019	CHROMagar	3,984,359	145,482	59
	F19-10-9	Oct-2019	LB	4,013,624	-	78
	F19-10-MH12	Oct-2019	Mueller-Hinton-agar	3,877,559	-	62

605

606 **TABLE S2.** BLAST outputs of pF14-11 coverage and percentage identity of plasmids or contigs
607 from close ST25 strains.

Strain	Sequence	Acession number	Coverage of pF14-11	Identity to pF14-11
VB82	pVB82_1	CP050386	97.00%	100.00%
HWBA8	pHWBA8_1	CP020596	96.00%	100.00%
40288-CIRI	p40288-CIRI	CP151689	100.00%	99.99%
CI107	pCI107	CP098522	100.00%	99.99%
UPAB1	pAB5	CP032216, CP032218, CP032219	65.00%	99.95%
16A1524	contigs	GCA_030377255	100.00%	100.00%
NM3	contigs	GCA_001007725	100.00%	100.00%
17021	contigs	GCA_022241165	99.00%	100.00%
AB23	contigs	GCA_023896455	87.00%	100.00%
741019	contigs	GCA_001007775	99.00%	99.99%
545_16	contigs	GCA_015536865	99.00%	99.99%
CCBH28244	contigs	GCA_015666535	98.00%	99.99%
Ab376	contigs	GCA_012524275	98.00%	99.99%
17A1904	contigs	GCA_020256045	97.00%	99.99%
A-71.198	contigs	GCA_009829555	94.00%	99.99%
18A2070	contigs	GCA_020256005	96.00%	99.98%
A15	contigs	GCA_014531345	99.00%	99.97%
2992	contigs	GCA_008709655	99.00%	99.95%
A-71.192	contigs	GCA_009829595	95.00%	99.87%
OIFC143	contigs	GCA_000278665	73.00%	99.13%
CI79	contigs	GCA_000516635	83.00%	99.12%
Naval18	contigs	GCA_000214965	82.00%	99.12%
107m	contigs	GCA_000493615	1.00%	74.98%

608

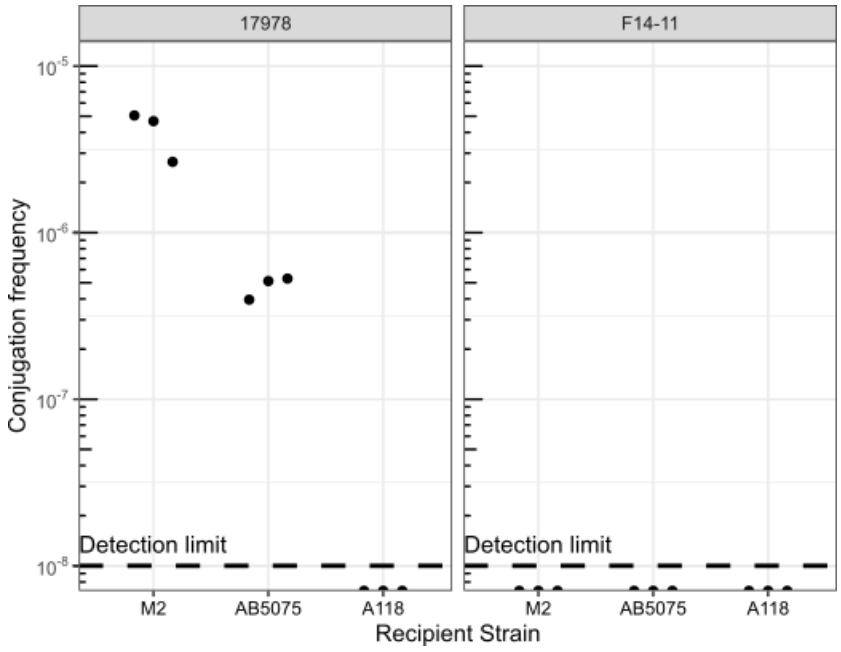

FIG S2 Conjugation frequencies between (left panel) *A. baumannii* strain 17978, carrying pAB3, or (right panel) strain F14-11, carrying pF14-11, and the recipient strains *Acinetobacter nosocomialis* M2, *A. baumannii* AB5075, or A118. Conjugation of pAB3 was used as control of conjugation conditions.

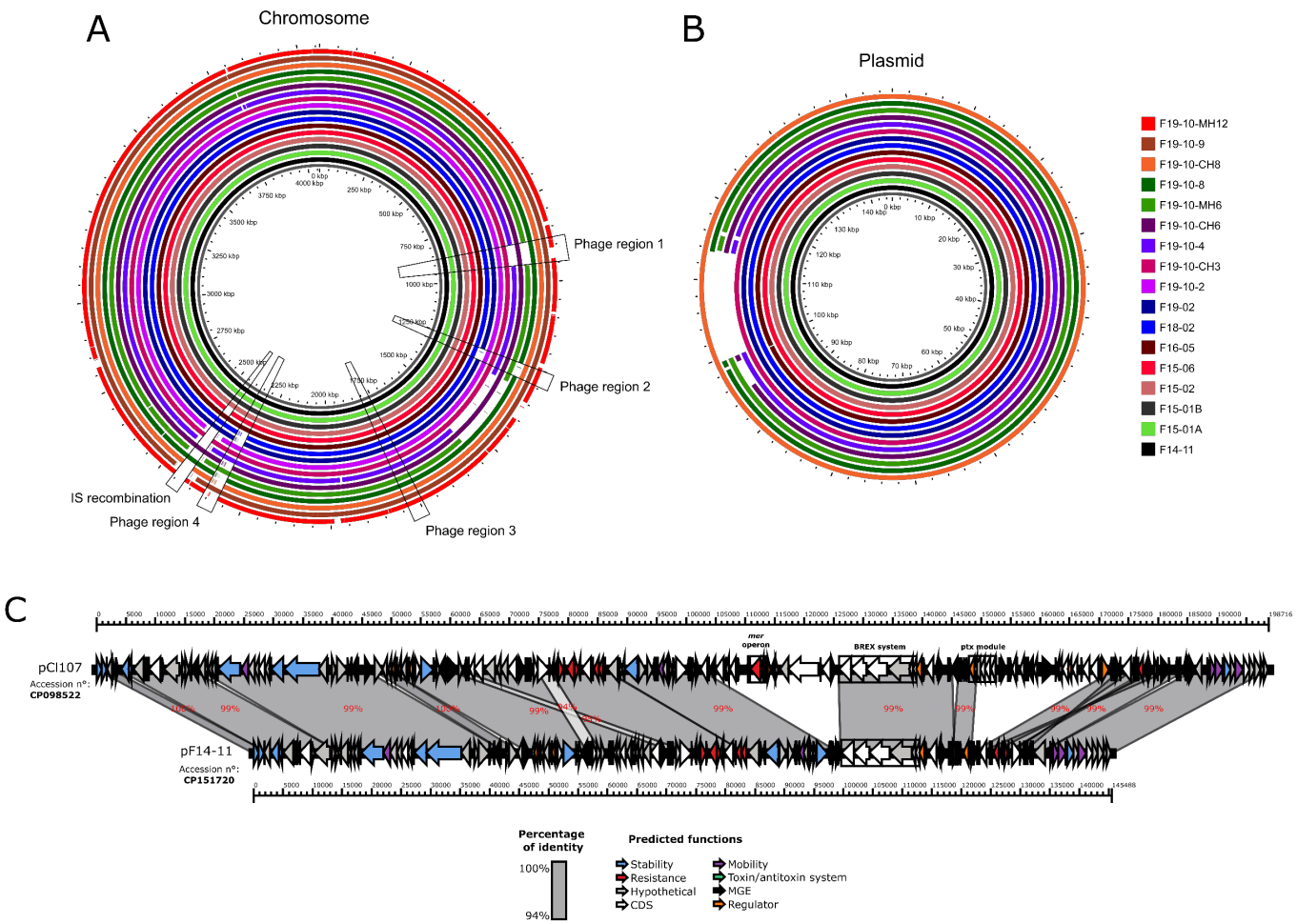

FIG S3 (A) Chromosome and (B) plasmid maps of the study strains using Gview. (C) Comparison of pF14-11 plasmid with pCI107 from CI107 strain revealing conserved and varying features with this well-described plasmid (27). Schematic representations are drawn to scale. Arrows represent open reading frames and prediction functions relevant to this study are indicated in the legend.

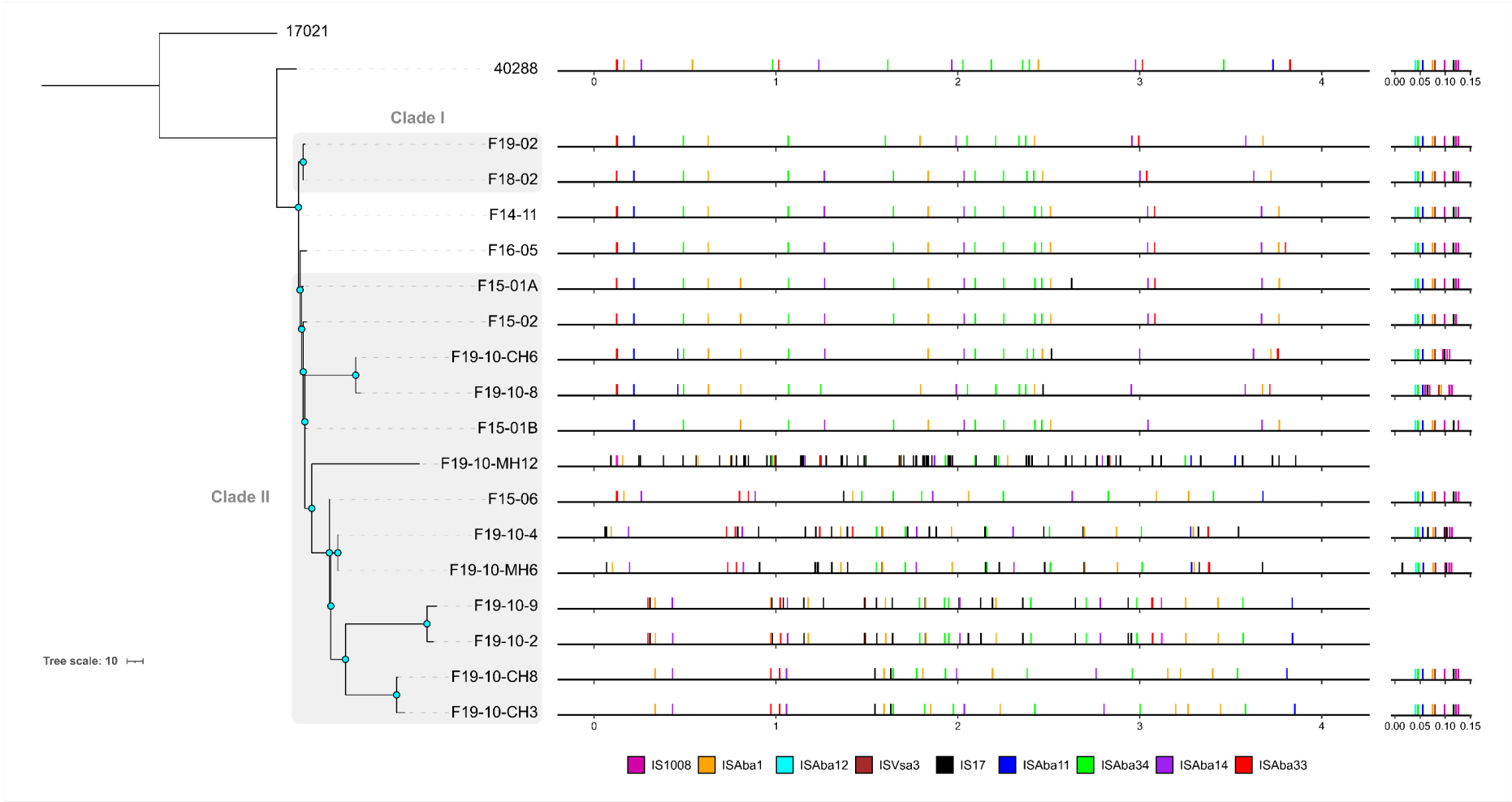

618

619 **Figure S4** Distribution of Insertion sequences in study strains and 40288 strain along their respective genomes associated with the phylogenetic
620 relationships. Blue nodes indicate bootstrap values >80.

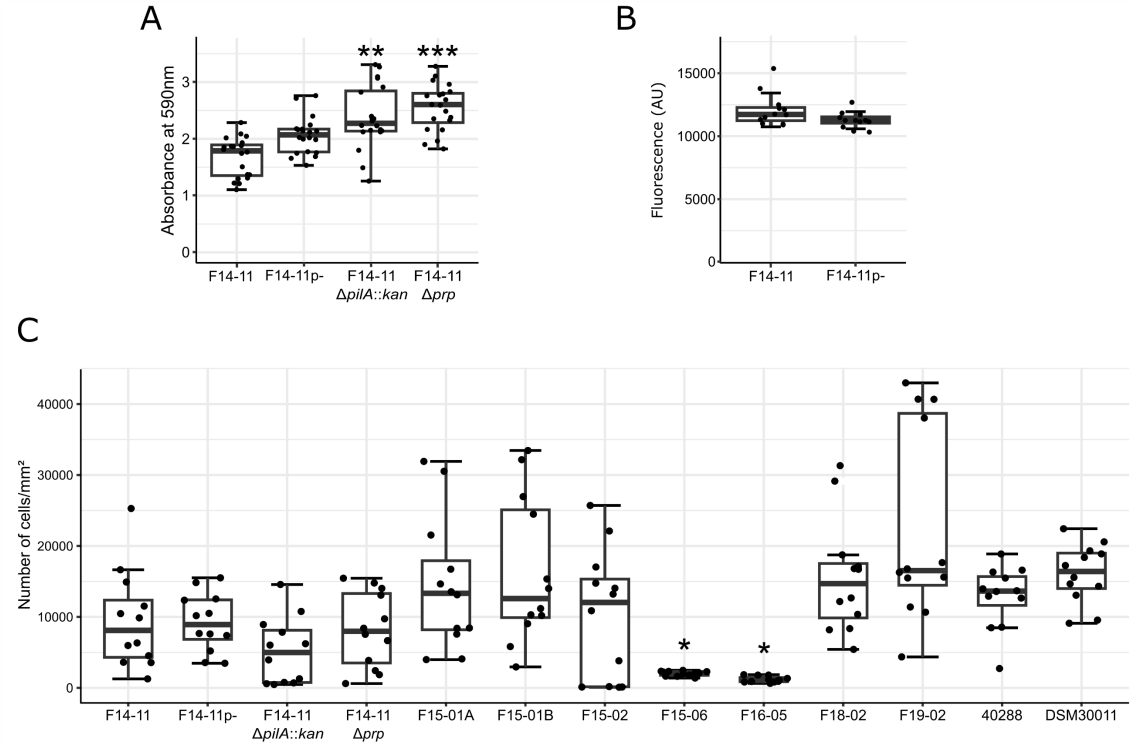

FIG S5. Adhesion and biofilm quantification. (A) Quantification of biofilm formation by F14-11 derivatives impaired for Type IV *pili* (Δ*pilA*::*kan*) or Prp type I *pili* (Δ*prp*) with crystal violet straining. (B) Congo red binding quantification of F14-11 wild-type and plasmid-less strains. (C) Adhesion quantification by the study strains, the dog UTI strain 40288 and the strong-adherent environmental strain DSM30011 after 1 hour of incubation using automatic cell counting in microscopy images. Error bars are generated from 12 replicas from 4 independent experiments. Statistically significant differences with F14-11 (Kruskal-Wallis rank-sum tests with Bonferroni-Holm correction) are highlighted with asterisks: (*) if the p-value < 0.05, (* *) if the p-value ≤ 0.01, and (* * *) if the p-value ≤ 0.001. The absence of asterisk indicates non-significant statistical difference.

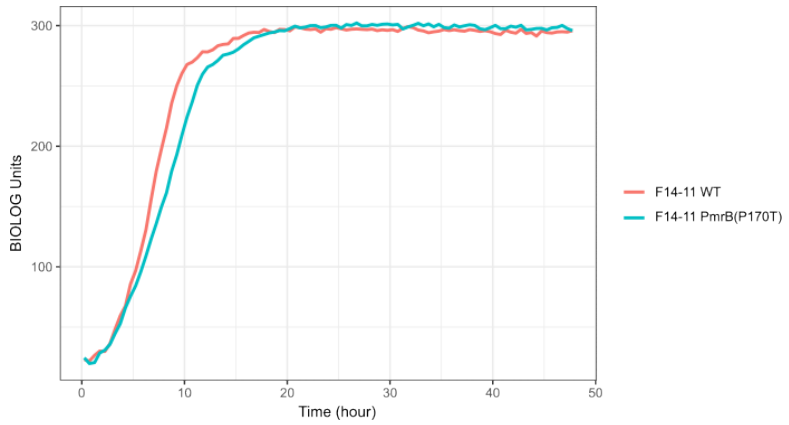

FIG S6. Growth curve of wild type F14-11 and its PmrB(P170T) derivative in rich medium (Biolog GenIII, control well)

634

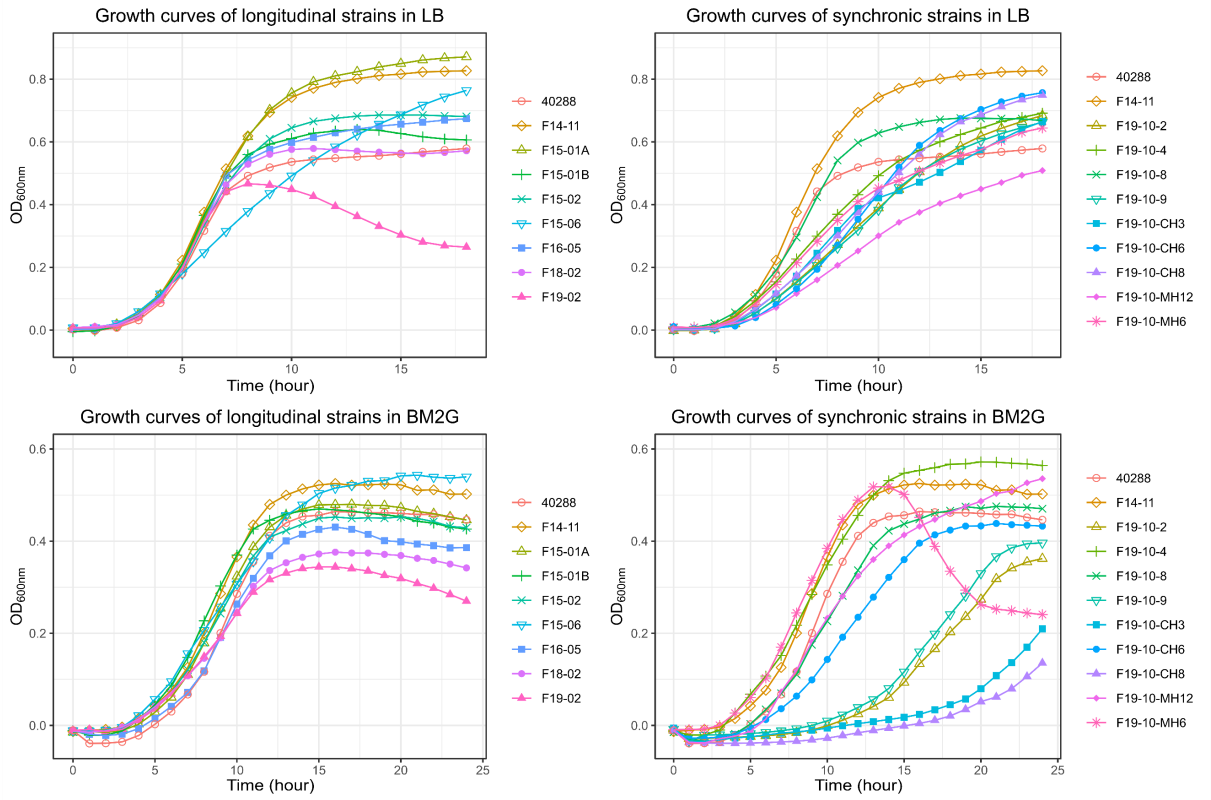

635

636 **FIG S7.** Growth rates of the longitudinal and synchronic strains in two different media (LB and
637 BM2G).

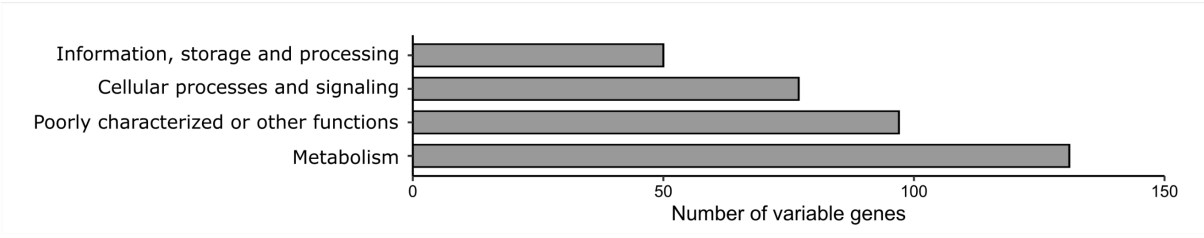

638

639 **FIG S8.** Distribution of functional categories of all the variable genes in comparison to F14-11.

640 **TABLE S3.** All the genetic variations identified in the study strains in comparison to the first
641 isolate (F14-11).

GENIC VARIATIONS						
Gene	Position	Strains	Size	Type	Support	Product
transposase gene	13,306	F19-10-4	601	deletion	Plasmid	transposase of ISAba34
transposition gene	18,898	F19-10-8	406 115	insertion deletion		transposition protein
transposition gene	19,309	F19-10-CH6	225	deletion		transposition protein
aacA-aphD	24,342	F19-02	982	insertion		Bifunctional AAC/APH
hypothetical	41,897	F19-10-CH3	1	snp		Unknown
hypothetical	57,130	F19-10-MH6	1052	insertion		Unknown
sasA	67,927	F19-10-8	1491	insertion		predicted cell-wall-anchored proteinsertionasA (LPXTG motif)
	67,928		246	deletion		
5S ribosomal RNA gene	23,503	F19-10-MH12	1	snp		5S ribosomal RNA
yliI	59,702	F19-10-2, F19-10-9	1	snp		glucose sorbosone dehydrogenase
hutC	80,540	F19-10-CH6, F19-10-8	1	snp		histidine utilization repressor
ABUW_0082	89,733	F19-10-CH6, F19-10-8	1	snp		X-Pro dipeptidyl-peptidase
	90,405	F19-10-9	1			
glmS	93,459	F16-05	1	snp		glutamine-fructose-6-phosphate transaminase (isomerizing)
xerD	152,569	F19-10-CH3, F19-10-CH8	1	snp		tyrosine recombinase XerD
rpoC	198,111	F19-10-CH6, F19-10-8	1	snp		DNA-directed RNA polymerase, beta' subunit
pcaU	227,170	F19-10-MH12	1	snp		transcriptional regulator, IclR family
recN	233,424	F19-10-MH12	2	deletion		DNA repair protein RecN
ABUW_3450	352,354	F19-10-MH12	1	snp		endonuclease / exonuclease / phosphatase
bfrD	399,565	F19-10-MH12	1	snp		Putative ferric siderophore receptor protein
macB	445,395	F19-10-MH12	1	snp		macrolide export ATP-binding / permease protein MacB
ABUW_3354	459,365	F16-05	1	snp		ggdef domain / eal domain protein
Transposase gene	467,027	F19-10-MH12	1	snp		Transposase
rsfS	529,063	F19-10-2, F19-10-9	1	snp		Ribosomal silencing factor RsfS
hyi	529,953	F19-10-2, F19-10-9	1	snp		hydroxypyruvate isomerase
panC	546,212	F19-10-2, F19-10-CH3, F19-10-CH8, F19-10-9	1	snp		pantoate-beta-alanine ligase
ABUW_3294	546,945	F19-10-MH12	1	snp		Nucleotide-binding protein
	546,954	F19-10-2, F19-10-CH3, F19-10-CH8, F19-10-9	2	insertion		
ohr	579,599	F19-10-CH3, F19-10-CH8	1	snp		Putative organic hydroperoxide resistance protein
filE	604,244	F19-10-CH6	1	snp		Pilus assembly protein FilE
rtsA	661,813	F19-10-2, F19-10-9	1	snp		Response regulator in two-component regulatory system with RstB
pleD	665,628	F19-10-2, F19-10-9	1	snp		Response regulator
yeiE	683,416	F19-10-2, F19-10-CH3, F19-10-CH8, F19-10-9	1	snp		transcriptionalregulator, LysR family
ABUW_3135	711,850	F19-10-2, F19-10-CH3, F19-10-CH8, F19-10-9	1	snp		cytochrome cassembly protein
rluB	733,600	F19-10-2, F19-10-9	1	snp		ribosomal large subunit pseudouridine synthase B
hypothetical	744,622	F19-10-2, F19-10-9	1	snp		Unknown
prs	748,345	F19-10-CH6, F19-10-8	1	snp		phosphoribosyl pyrophosphate synthetase
ABUW_3090	750,782	F18-02, F19-02	1	snp		O-linked N-acetylglucosamine transferase OGT
	750,788		1			
algC	803,644	F19-10-MH12	1	snp		phosphomannomutase
ABUW_3039	805,669	F19-10-2, F19-10-9	1	snp		GNAT family N-acetyltransferase
fur	810,016	F19-10-MH12	1	snp		ferricuptake regulation protein
pilT	811,917	F19-10-MH12	1	snp		twitching mobility protein
emrB	825,802	F19-10-MH12	1	snp		multidrug resistance protein B
yejK	884,399	F19-10-CH3, F19-10-CH8	1	snp		Nucleoid-associated protein YejK
mcpII	944,588	F19-10-MH12	1	snp		glyoxalase
catD	948,534	F19-10-2, F19-10-9	1	snp		putative hydrolase
cysN	1,006,449	F19-10-MH12	1	snp		sulfate adenylyltransferase subunit 1
rsmD	1,021,880	F19-10-9	1	snp		Ribosomal RNA small subunit methyltransferase D
pepP	1,040,770	F19-10-CH3, F19-10-CH8	1	snp		X-Pro aminopeptidase
mltD	1,057,383	F19-10-9	1	snp		lytic transglycosylase
	1,057,757		1			
	1,058,096	F19-10-CH3, F19-10-CH8	1			
hypothetical	1,092,091	F19-10-CH6, F19-10-8	1	snp		Unknown
calB	1,114,615	F19-10-CH3, F19-10-CH8	1	snp		aldehyde dehydrogenase
hcaK	1,136,699	F15-01B, F15-02, F15-06, F19-10-2, F19-10-CH3, F19-10-4, F19-10-CH6, F19-10-MH6, F19-10-8, F19-10-CH8, F19-10-9, F19-10-MH12	1	snp		3-hydroxyphenylpropionic acid transporter
hcaR	1,137,422	F19-10-CH6, F19-10-8	1	snp		transcriptional regulator, MarR-family
benP2	1,141,071	F19-10-CH3, F19-10-CH8	1	snp		benzoate transport porin BenP
hapE	1,163,317	F19-10-4, F19-10-MH6	1	snp		Putative flavin-binding monooxygenase
csrA	1,169,719	F19-10-CH6, F19-10-8	1	snp		carbon storage regulator
alaS	1,171,454	F19-10-2, F19-10-9	1	snp		alanyl-tRNA synthetase
	1,173,440	F19-10-CH6, F19-10-8	1			
ABUW_2740	1,181,914	F15-06	2	deletion		OsmC-like protein
pyrX	1,192,159	F19-10-CH3	1	snp		dihydroorotase
hypothetical	1,266,110	F19-10-MH12	2	insertion		Unknown
lptB	1,299,034	F19-10-MH12	1	snp		ABC transporter, ATP-binding protein
cyaD	1,303,869	F19-10-MH12	1	snp		membrane spanning export protein
	1,304,086	F19-10-CH6, F19-10-8	1			
	1,304,091	F15-01B	1			
ybiF	1,313,214	F19-10-CH3, F19-10-CH8	1	snp		inner membrane transport protein YbiF
ybgK	1,331,800	F19-10-MH12	1	snp		allophanatehydrolase
ABUW_2582	1,361,019	F19-10-2, F19-10-9	1	snp		DUF4440 domain-containing protein
icmF	1,382,155	F19-10-CH6, F19-10-8	1	snp		typeVI secretion protein IcmF
dcaS	1,473,682	F19-10-2, F19-10-9	1	snp		transcriptional regulator, IclR family
ABUW_2322	1,641,301	F19-10-MH12	2	deletion		phage integrase
papC	1,650,401	F19-10-2, F19-10-9	1	snp		fimbrial protein
ABUW_2302	1,660,771	F19-10-2, F19-10-9	1	snp		transcriptional regulator, XRE family
ABUW_2270	1,692,643	F19-02	1	snp		Lipoprotein
ostA	1,696,163	F19-10-2	1	snp		organic solvent tolerance protein
gspK	1,712,003	F19-10-CH6, F19-10-8, F19-10-MH12	1	snp		general secretion pathway protein K
hibcH	1,712,364	F19-10-MH12	1	snp		Enoyl-CoA hydratase
	1,714,219	F19-10-MH12	1			
	1,732,617	F19-10-CH6, F19-10-8	1			
ppiD	1,765,571	F19-10-2, F19-10-9	1	snp		peptidyl-prolyl cis-trans isomerase
acoA	1,875,749	F19-10-CH3	1	snp		acetoin:2,6-dichlorophenolindophenol oxidoreductase alpha subunit
gltC	1,914,659	F19-10-CH3, F19-10-CH8	1	snp		transcriptionalregulator, LysR family
hypothetical	1,955,643	F19-10-8	1	snp		Unknown
cupC	1,959,422	F15-01B, F15-06, F19-10-2, F19-10-CH3, F19-10-CH6, F19-10-MH6, F19-10-8, F19-10-CH8, F19-10-9, F19-10-MH12	2	deletion		outer membranefimbrial usher protein
	1,960,690	F15-02	2			
	1,961,307	F16-05	2			
msbA	1,976,399	F19-10-CH3, F19-10-CH8	1	snp		lipidA export permease/ATP-binding protein MsbA
ssuA	1,991,149	F19-10-MH12	5	complex		Sulfonate / nitrate / taurine transport system substrate-binding protein
ssuD	1,991,829	F19-10-CH3, F19-10-CH8	1	snp		alkanesulfonate monooxygenase
	2,002,880	F19-10-MH12	1			
oruR	2,014,835	F19-10-MH12	1	snp		AraC family transcriptional regulator
ABUW_1936	2,055,079	F19-10-CH3, F19-10-CH8	1	snp		transcriptionalregulator, LysR family
ABUW_1935	2,056,094	F19-10-2, F19-10-9	2	deletion		fumarylacetoacetate hydrolase
	2,056,237	F19-10-CH6, F19-10-8	1	snp		
ABUW_1924	2,076,802	F19-10-CH6, F19-10-8, F19-10-MH12	3	deletion		transcriptionalregulator, GntR family
	2,077,250	F19-10-2, F19-10-CH3, F19-10-CH8, F19-10-9	1	snp		
hypothetical	2,090,336	F19-10-8	2	deletion		Unknown

642

gpmA	2,125,323	F19-10-2, F19-10-CH3, F19-10-4, F19-10-MH6, F19-10-CH8, F19-10-9	1	snp		2,3-bisphosphoglycerate-dependent phosphoglycerate mutase
ABUW_1883	2,129,382	F19-10-2, F19-10-9	1	snp		FAH family protein
ABUW_1861	2,152,327	F19-10-MH12	1	snp		ringhydroxylating dioxygenase, Rieske
pyrG	2,189,133	F15-01A, F15-01B, F15-02, F15-06, F19-10-2, F19-10-CH3, F19-10-4, F19-10-CH6, F19-10-MH6, F19-10-8, F19-10-CH8, F19-10-9, F19-10-MH12	1	snp		CTP synthase
ABUW_1800	2,216,179	F19-10-2, F19-10-9	1	snp		ferrichrome-iron receptor
	2,216,267		1			
	2,217,382		1			
yqiJ	2,219,489	F19-10-CH3	1	snp		Inner membrane protein YqiJ
hypothetical	2,220,185	F19-10-MH12	1	snp		Inner membrane protein
cydA	2,220,207	F19-10-2, F19-10-CH3, F19-10-CH8, F19-10-9	1	snp		cytochrome D ubiquinol oxidase subunit I
hypothetical	2,230,585	F19-10-2, F19-10-9	1	snp		Unknown
ykoW	2,245,494	F19-10-2, F19-10-CH3, F19-10-CH8, F19-10-9	2	deletion		Diguanylate cyclase / phosphodiesterase with PAS / PAC sensor(S)
rimO	2,277,589	F19-10-2, F19-10-9	1	snp		Ribosomal protein S12 methyl thiotransferase RimO
accB	2,315,146	F19-10-MH12	1	snp		acetyl-CoA carboxylase, biotin carboxyl carrier protein
ABUW_1695	2,316,804	F19-10-CH6, F19-10-8	1	snp		Signal peptide protein
gbsB	2,373,908	F19-10-2, F19-10-9	1	snp		Choline dehydrogenase
dnaX	2,377,861	F19-10-CH6, F19-10-8	1	snp		DNA polymerase III subunit gamma/tau
	2,378,410	F19-10-8	1			
ABUW_1637	2,472,470	F19-10-2, F19-10-CH3, F19-10-CH8, F19-10-9	1	snp		oxidoreductase short-chain dehydrogenase/reductase family
ABUW_1605	2,503,139	F19-10-8	1	snp		RNA pseudo uridine synthase family protein
ABUW_1600	2,505,970	F19-10-CH3, F19-10-CH8	1	snp		UPF0756 membrane protein A15_2121
pgaD	2,552,659	F19-10-MH12	1	snp		Poly-beta-1,6-N-acetyl-D-glucosamine biosynthesis protein PgaD
pgaC	2,553,475	F19-10-MH12	1	snp		glycosyl transferase, family 2 protein
	2,553,959	F19-10-2, F19-10-9	2	insertion		
pgaB	2,555,101	F16-05	1	snp		polysaccharide deacetylase
	2,555,580	F19-10-MH12	1			
	2,555,659	F15-01B, F15-06, F19-10-2, F19-10-CH3, F19-10-4, F19-10-CH6, F19-10-MH6, F19-10-CH8, F19-10-9, F19-10-MH12	1			
	2,555,743	F19-10-MH12	1			
nahR	2,595,267	F19-10-CH8	1	snp		transcriptional regulator, LysR family
csuB	2,621,526	F19-10-MH12	2	deletion		type I pilus protein CsuB
	2,621,655	F19-10-2, F19-10-9	1	snp		
ABUW_1456	2,665,131	F19-10-CH3, F19-10-CH8	1	snp		patatin family phospholipase
rpsU	2,670,130	F19-10-2	1	snp		ribosomal protein S21
ABUW_1447	2,675,030	F19-10-MH12	1	snp		Peptidase_M48 domain-containing protein
ABUW_1350	2,719,436	F19-10-CH3, F19-10-CH8	1	snp		DUF4010 domain-containing protein
metF	2,767,892	F19-10-2, F19-10-9	1	snp		5,10-methylene tetrahydrofolate reductase
dtpT	2,785,448	F19-10-MH12	1	snp		dipeptide / tripeptide permease
ABUW_1184	2,816,665	F19-10-2, F19-10-9	1	snp		ABC transporter, ATP-binding protein
basG	2,818,236	F19-10-MH12	1	snp		histidine decarboxylase
bauA	2,826,283	F19-10-CH6, F19-10-8	1	snp		ferric acinetobactin receptor
	2,826,654	F19-10-2, F19-10-9	1			
basB	2,832,231	F19-10-CH6, F19-10-8	1	snp		non-ribosomal peptide synthetase
efp	2,850,743	F19-10-CH6, F19-10-8	1	snp		translation elongation factor P
ABUW_1136	2,857,347	F19-10-MH12	1	snp		sodium / bile acid symporter family protein
aroP3	2,882,913	F19-10-CH6, F19-10-8	1	snp		aromatic amino acid transport protein
ABUW_1111	2,886,388	F19-10-CH3, F19-10-CH8	1	snp		aldehyde dehydrogenase
icaA	2,939,211	F19-10-MH12	3	insertion		N-acetylglucosaminyl transferase
proB	2,950,528	F19-10-2	1	snp		glutamate 5-kinase
pabC	2,980,993	F19-10-MH12	1	snp		aminodeoxychorismate lyase
purL	2,996,955	F19-10-MH12	1	snp		phosphoribosyl formyl glycinamidine synthase
comA	3,027,183	F19-10-CH3, F19-10-CH8	1	snp		competence factor involved in DNA uptake
ABUW_0967	3,036,275	F19-10-CH6, F19-10-8	1	snp		putative RND family drug transporter
ABUW_0949	3,057,779	F19-10-2, F19-10-9	1	snp		hypothetical
hypothetical	3,069,429	F19-10-CH6, F19-10-8	1	snp		Unknown
ABUW_2539	3,081,722	F19-10-CH6, F19-10-8	1	snp		transposase inhibitor
vlI	3,085,622	F19-10-CH3, F19-10-CH8	1	snp		lytic transglycosylase, catalytic
ftsH	3,112,575	F19-10-MH12	1	snp		cell division protein FtsH
ABUW_0897	3,114,621	F19-10-MH12	1	snp		Putative RNA-binding protein
bapA	3,133,668	F15-01B, F15-02, F15-06, F19-10-2, F19-10-CH3, F19-10-4, F19-10-CH6, F19-10-MH6, F19-10-8, F19-10-CH8, F19-10-9, F19-10-MH12	1	snp		Biofilm-associated protein BapA
sucA	3,149,032	F19-10-2, F19-10-9	1	snp		oxoglutarate dehydrogenase (succinyl-transferring)
hypothetical	3,155,706	F19-10-CH6, F19-10-8	2	deletion		Unknown
ispB	3,174,686	F19-10-2, F19-10-9	1	snp		trans-hexaprenyl transtransferase
hypothetical	3,189,844	F19-10-2	1	snp		Unknown
ABUW_0830	3,195,458	F19-10-MH12	1	snp		hypothetical
pmrB	3,196,703	F15-01A, F15-01B, F15-02, F15-06, F16-05, F19-10-2, F19-10-CH3, F19-10-4, F19-10-CH6, F19-10-MH6, F19-10-8, F19-10-CH8, F19-10-9, F19-10-MH12	1	snp		Histidine kinase PmrB
	3,197,091	F19-10-MH12	1			
	3,197,092	F19-10-CH3, F19-10-CH8	1			
hchA	3,211,313	F19-10-MH12	1	snp		chaperone protein
fimT	3,295,357	F19-10-2, F19-10-9	1	snp		type 4 fimbrial biogenesis protein FimT
yhjE	3,314,081	F19-10-CH3, F19-10-CH8	1	snp		metabolite transport protein
accD	3,324,051	F19-10-4, F19-10-MH6	1	snp		acetyl-CoA carboxylase, carboxyl transferase, beta subunit
psaB	3,399,155	F19-10-MH12	1	snp		OmpA / MotB
slt	3,437,614	F19-10-9	1	snp		lytic transglycosylase, catalytic
ABUW_0439	3,463,037	F19-10-2, F19-10-CH3, F19-10-4, F19-10-MH6, F19-10-CH8, F19-10-9	2	deletion		rhomboid family peptidase
rpoA	3,470,211	F19-10-2, F19-10-CH3, F19-10-CH8, F19-10-9	1	snp		DNA-directed RNA polymerase, alpha subunit
deaD	3,505,789	F19-10-CH6, F19-10-8, F19-10-MH12	1	snp		DEAD / DEAH boxhelicase
	3,505,798		1			
ABUW_0375	3,514,048	F19-10-MH12	1	snp		Signal peptide
mmgC	3,517,179	F18-02	2	deletion		acyl-CoA dehydrogenase
ydfC	3,529,243	F19-10-MH12	1	snp		Transporter, 10 TMS drug/metabolite exporter (DME) family
mmuP	3,544,178	F16-05	1	snp		Putative APC family, S-methylmethionine transporter (MmuP)
gltB	3,592,561	F19-10-CH6, F19-10-8	1	snp		glutamate synthase, large subunit
ftsI	3,612,362	F15-01A	1	snp		Peptidoglycan D,D-transpeptidase FtsI
	3,612,574	F15-02	1			
ABUW_0244	3,656,360	F19-10-MH12	1	snp		DMT family transporter
hypothetical	3,675,302	F19-10-CH6, F19-10-8	2	insertion		Unknown
gabP	3,697,271	F19-10-CH3, F19-10-CH8	1	snp		GABA permease
	3,697,332	F19-10-CH6, F19-10-8	1			
ABUW_0172	3,731,075	F19-10-2, F19-10-9	1	snp		Ribosomal RNA small subunit methyltransferase E
guaB	3,742,122	F19-10-CH3, F19-10-CH8	1	snp		inosine-5'-monophosphate dehydrogenase
hypothetical	3,795,707	F19-10-CH3, F19-10-CH8	1	snp	Chromosome	Unknown
argS	3,886,237	F19-10-CH3, F19-10-CH8	1	snp		arginyl-tRNA synthetase
ABUW_3773	3,915,008	F19-10-CH3, F19-10-CH8	1	snp		acyl-CoA synthetase / AMP-acid ligase
dadA2	3,934,669	F19-10-MH12	1	snp		D-amino acid dehydrogenase small subunit
foxA	3,937,460	F19-10-CH3, F19-10-CH8	1	snp		Putative ferrichrome-iron receptor protein
lldD	3,967,179	F19-10-2, F19-10-9	1	snp		L-lactate dehydrogenase (cytochrome)
hypothetical	3,981,476	F18-02, F19-02	1	snp		Unknown
ptk	3,990,566	F19-10-2, F19-10-9	1	snp		tyrosine-protein kinase
5S ribosomal RNA gene	4,023,726	F19-10-MH12	1	snp		5S ribosomal RNA

ABUW_3890	4,047,894	F19-10-CH6, F19-10-8	1	snp	PAP2 superfamily protein
guaD2	4,052,990	F19-10-2, F19-10-9	1	snp	guanine deaminase
czcD	4,056,163	F15-02, F19-10-2, F19-10-CH3, F19-10-CH8, F19-10-9	6	deletion	Cation efflux protein
		F19-10-CH6, F19-10-8	7	insertion	
5S ribosomal RNA gene	23,447	F19-10-MH6	5797	deletion	5S ribosomal RNA
	23,474	F19-10-4			
ABUW_0082	89,766	F19-10-MH12	1692	deletion	X-Pro dipeptidyl-peptidase
cbbZ	91,458	F19-10-MH12	1002	insertion	haloacid dehydrogenase
transposase gene	121,183	F19-10-9	4662	insertion	Transposition protein
			6799	deletion	
	121,233	F19-10-2	4612	insertion	
			6602	deletion	
hypothetical	127,836	F19-10-2	8448	deletion	Unknown
	127,878		95	insertion	
	127,974		95	deletion	
hypothetical	137,309	F19-10-CH6	3753	deletion	Unknown
hypothetical	139,761	F19-10-4	1052	insertion	Unknown
hypothetical	140,656	F19-10-8	823	insertion	Unknown
	140,871	F16-05	191	deletion	
hvrA	176,884	F19-10-4	1040	insertion	Putative DNA binding protein
	176,888	F19-10-MH6	1051		
sel-1	393,824	F18-02, F19-02	9	deletion	Sel1 domain protein
ggdef	457,967	F19-10-MH12	1110	insertion	ggdef domain/eal domain protein
	457,971	F19-10-CH6, F19-10-8			
hypothetical	562,292	F19-10-MH12	12	deletion	Lipoprotein
filE	604,179	F16-05, F19-10-CH6	67	deletion	Putative pilus assembly protein FilE
	604,180	F19-10-9	40	insertion	
	604,181	F19-10-8	9	insertion	
	604,201	F19-10-MH6	31	insertion	
	604,234	F19-10-CH8	30	insertion	
	604,240	F15-01B	9	insertion	
	604,249	F15-02	9	insertion	
	604,257	F15-01A	9	insertion	
	604,277	F18-02	9	insertion	
	604,305	F19-10-2	39	insertion	
		F19-10-CH3, F19-10-4	30		
	604,306	F15-06	9	insertion	
		F19-10-CH8	17495		
argJ	621,802	F19-10-CH8	17495	deletion	glutamate N-acetyltransferase / amino-acid acetyltransferase
add2	623,956	F19-10-CH3, F19-10-CH8	116	deletion	adenosine deaminase
		F19-10-MH6	60		
hypothetical	744,307	F19-10-MH12	1052	insertion	Unknown
algC	803,168	F15-01A, F15-01B, F15-02, F19-10-CH6, F19-10-8	1193	insertion	phosphomannomutase
	803,174	F19-10-2, F19-10-CH3, F19-10-4, F19-10-MH6, F19-10-CH8, F19-10-9	1193	insertion	
	803,175	F15-06	1194	insertion	
	803,180	F19-10-MH12	1194	insertion	
ABUW_3037	807,301	F19-10-4, F19-10-MH6	1052	insertion	Hemerythrin domain-containing protein
	807,319	F19-10-MH12	1051	insertion	
hypothetical	833,535	F19-10-MH12	11423	deletion	Unknown
hypothetical	870,850	F19-10-CH3, F19-10-CH8	1193	insertion	Unknown
hypothetical	884,630	F19-10-MH12	516	deletion	Unknown
	885,146	F19-10-MH12	1013	insertion	
hypothetical	885,883	F19-10-MH12	1052	insertion	Unknown
ABUW_2985	907,272	F19-10-MH12	30114	deletion	TonB-dependent receptor
pgaC	937,386	F19-10-MH12	1043	insertion	Poly-beta-1,6-N-acetyl-D-glucosamine synthase
pecR	948,961	F19-10-4, F19-10-MH6	73474	deletion	Beta-ketoacyl-ACP reductase
pfeA	982,519	F19-10-2	21364	insertion	TonBdependent outer membrane siderophore receptor protein
		F19-10-9	21165		
rubA	998,871	F19-10-9	16351	deletion	rubredoxin
ABUW_2861	1,037,789	F19-10-MH12	1052	insertion	hypothetical
mltD	1,057,355	F19-10-MH12	1052	insertion	lytic transglycosylase
atsA	1,080,074	F19-10-MH12	1193	insertion	arylsulfatase
HP	1,096,794	F19-10-2	1051	insertion	Transcriptional regulator
	1,096,796	F19-10-MH12	1041	insertion	
ABUW_2705	1,230,820	F19-10-MH12	12815	deletion	hypothetical
proC	1,241,521	F19-10-8	8406	insertion	pyrroline-5-carboxylate reductase
ABUW_2685	1,243,635	F19-10-MH12	1041	insertion	hypothetical
hypothetical	1,256,758	F19-10-MH12	1052	insertion	Unknown
ABUW_2653	1,293,601	F19-10-CH3	19467	insertion	shufflon-specific DNA recombinase
		F19-10-CH8	19516		
	1,293,612	F19-10-2, F19-10-4, F19-10-MH6, F19-10-9, F19-10-CH3, F19-10-CH8	8	deletion	
hypothetical	1,341,918	F19-10-2, F19-10-9	1316	insertion	Unknown
ABUW_2556	1,400,247	F19-10-MH12	1041	insertion	hypothetical
soxR	1,400,919	F19-10-2	262	deletion	redox-sensitive transcriptional activator SoxR
	1,400,923	F19-10-9	1052	insertion	
ABUW_1958	1,431,155	F19-10-MH12	1052	insertion	type III restriction enzyme, res subunit
	1,431,709	F19-10-MH12	2002	deletion	
	1,433,711	F19-10-MH12	1043	insertion	
ABUW_2442	1,513,372	F19-10-MH12	1052	insertion	hypothetical
ABUW_2437	1,516,227	F19-10-MH12	1052	insertion	hemeoxygenase-like protein
ABUW_2434	1,520,631	F19-10-MH12	1024	insertion	hypothetical
srpH	1,546,226	F19-10-MH12	1052	insertion	serine acetyltransferase
gltC	1,551,140	F19-10-4, F19-10-MH6	232689	deletion	transcriptional regulator, LysR family
ABUW_2325	1,638,208	F19-10-MH12	1052	insertion	transcriptionalregulator, TetR family
ABUW_2316	1,647,333	F19-10-MH12	1051	insertion	hypothetical
mrkC	1,651,613	F19-10-4, F19-10-MH6	1052	insertion	fimbrial biogenesis outer membrane usher protein
cobC	1,830,823	F19-10-MH12	354	deletion	fructose-2,6-bisphosphatase
ABUW_2172	1,831,177	F19-10-MH12	1027	insertion	histidine acid phosphatase family protein
ABUW_2167	1,838,443	F19-10-MH12	1639	deletion	iron-regulated membrane protein
ABUW_2165	1,840,082	F19-10-MH12	1008	insertion	outer-membranereceptor for Fe(III)-coprogen,Fe(III)-ferrioxamine B and Fe(III)-rhodotrulic acid
	1,840,101	F19-10-MH12	7	deletion	
ABUW_2155	1,854,392	F19-10-MH12	1051	insertion	hypothetical
ABUW_2154	1,854,801	F19-10-9	1052	insertion	hypothetical
ABUW_2058	1,955,625	F19-10-MH12	1052	insertion	hypothetical
hypothetical	1,955,674	F19-10-4	1043	insertion	Unknown
cupA	1,962,301	F15-01A, F15-02, F19-10-MH12	150	deletion	Fimbrial subunit
	1,962,302	F15-01B, F16-05, F19-10-CH6, F19-10-8	149	deletion	
	1,962,452	F15-06, F19-10-CH8	149	deletion	
		F19-10-2, F19-10-CH3, F19-10-MH6, F19-10-9	150		
hypothetical	1,963,435	F19-10-4	7760	deletion	Unknown
gsiA	1,972,590	F19-10-MH12	18552	deletion	glutathione import ATP-binding protein GsiA
tatC	1,986,634	F19-10-2	1052	insertion	twin arginine-targeting protein translocase TatC
ssuA	1,991,142	F19-10-MH12	1028	insertion	Sulfonate / nitrate / taurine transport system substrate-binding protein
fyuA	2,000,304	F19-10-MH12	1052	insertion	Receptor-mostly Fe transport
emrA	2,036,586	F19-10-9	1052	insertion	Colistin resistance protein EmrA
hypothetical	2,082,044	F19-10-4	1052	insertion	Unknown
aes	2,107,724	F19-10-MH12	1052	insertion	Acetyl esterase
ABUW_1885	2,110,258	F19-10-MH12	1052	insertion	hypothetical
katE	2,112,175	F19-10-2, F19-10-9	301	deletion	catalase
calB	2,115,730	F19-10-2, F19-10-9	1314	insertion	aldehyde dehydrogenase
pcaD1	2,178,639	F19-10-9	40	insertion	3-oxoadipate enol-lactonase
	2,178,680	F19-10-2	40	insertion	
ABUW_1797	2,219,383	F19-10-4, F19-10-MH6	1052	insertion	hypothetical

[illegible]	2,219,432	F19-10-2, F19-10-9	1052	insertion	hypothetical
ABUW_1758	2,255,937	F19-10-MH12	1052	insertion	hypothetical
hcaT	2,318,396	F19-10-CH6	43149	deletion	metabolite transporter, MFS superfamily
		F19-10-CH8	6	insertion	
	2,318,417	F18-02, F19-02, F19-10-8, F19-10-MH12	43128	deletion	
dnaX	2,377,932	F19-10-4	19	insertion	DNA polymerase III subunit gamma/tau
	2,377,990	F19-10-MH12	6	deletion	
	2,378,011	F16-05	6	deletion	
	2,378,019	F19-10-2, F19-10-9	19	insertion	
	2,378,043	F19-10-MH6	12	insertion	
	2,378,044	F19-10-CH6, F19-10-8	6	insertion	
	2,378,071	F19-10-CH3, F19-10-CH8	6	insertion	
cpaA	2,381,061	F19-10-4	1192	insertion	Metallo endopeptidase CpaA
ABUW_1664	2,399,317	F19-10-2, F19-10-9	1044	insertion	RDD domain-containing protein
ABUW_1655	2,406,886	F19-10-MH12	3352	deletion	TonB-dependent siderophore receptor
ABUW_1653	2,408,637	F19-10-4	1044	insertion	hypothetical
ABUW_3471	2,423,209	F19-10-MH12	36623	deletion	Hca operon transcriptional activator
hypothetical	2,453,180	F19-10-8	2272	deletion	Unknown
	2,453,375	F19-10-CH6	2272	deletion	
transposase gene	2,459,732	F19-10-CH3, F19-10-CH8	37831	deletion	Transposase
	2,459,734	F15-06	37833	deletion	
ABUW_1637	2,472,269	F19-10-2, F19-10-9	72951	deletion	oxidoreductase short-chain dehydrogenase / reductase family
		F19-10-4	63631		
		F19-10-MH6	64327		
	2,472,276	F19-10-CH3, F19-10-CH8	1051	insertion	
pgaB	2,554,579	F19-10-8	3786	deletion	polysaccharide deacetylase
pgaA	2,558,042	F19-10-CH6	312	deletion	Outer membrane protein
	2,558,084	F19-10-4, F19-10-MH6	1029	insertion	
ABUW_1499	2,610,036	F19-10-MH12	1052	insertion	hypothetical
csuC	2,620,461	F19-10-9	1042	insertion	Csu fimbrial biogenesis chaperone CsuC
	2,621,028	F19-10-9	566	deletion	
	2,621,033	F19-10-2	1050	insertion	
csuB	2,621,577	F19-10-MH12	1052	insertion	type I pilus protein CsuB
	2,621,582	F19-10-2	1052	insertion	
csuA/B	2,622,319	F19-10-MH12	1052	insertion	Fimbrial major subunit CsuA/B family protein
	2,622,731	F15-06, F19-10-2, F19-10-CH3, F19-10-4, F19-10-MH6, F19-10-CH8, F19-10-9	1193	insertion	
ABUW_1486	2,623,440	F19-10-MH12	1042	insertion	transcriptional regulator, TetR family protein
ABUW_1473	2,631,199	F19-10-MH6	1052	insertion	hypothetical
ABUW_1466	2,635,994	F19-10-MH6	1052	insertion	hypothetical
hypothetical	2,646,033	F19-10-MH6	1044	insertion	Unknown
hypothetical	2,649,909	F19-10-MH6	3875	deletion	Unknown
qacF	2,726,238	F19-10-MH12	1052	insertion	small multidrug resistance protein
basE	2,819,564	F19-10-MH12	24830	deletion	2,3-dihydroxybenzoate-AMP ligase
hypothetical	2,844,394	F19-10-MH12	1053	insertion	Unknown
hypothetical	2,847,076	F19-10-9	1052	insertion	Unknown
	2,847,080	F19-10-MH12	1052	insertion	
pstB	2,877,440	F19-10-MH12	1558	deletion	phosphate ABC transporter, ATP-binding protein
pstA	2,878,998	F19-10-MH12	1039	insertion	phosphate ABC transporter, permease protein
hypothetical	2,952,824	F19-10-2, F19-10-9	1052	insertion	Unknown
	2,953,216	F19-10-MH12	1052	insertion	
ABUW_0985	3,014,384	F19-10-MH12	1051	insertion	hypothetical
ABUW_0984	3,017,720	F19-10-MH12	1052	insertion	hypothetical
hypothetical	3,071,839	F19-10-MH12	1051	insertion	Unknown
ABUW_0896	3,115,299	F19-10-MH12	1052	insertion	hypothetical
hypothetical	3,126,118	F19-10-2, F19-10-9	1052	insertion	Unknown
bapA	3,127,303	F19-10-2, F19-10-9	3380	insertion	Biofilm-associated protein BapA
	3,128,926	F15-06, F19-10-CH3, F19-10-4, F19-10-MH6, F19-10-CH8, F19-10-9	1193	insertion	
		F19-10-2	5554		
	3,131,312	F16-05	615	deletion	
	3,132,928	F19-10-4, F19-10-MH6	1839	deletion	
	3,133,292	F19-10-2	4365	deletion	
	3,133,337	F19-10-2	57	insertion	
	3,133,395	F19-10-2	57	deletion	
	3,134,475	F15-02	1876	deletion	
	3,135,478	F19-10-2, F19-10-4, F19-10-9	628	deletion	
	3,136,414	F15-06, F19-10-CH3, F19-10-MH6, F19-10-CH8	628	deletion	
ABUW_0588	3,359,389	F19-10-MH12	1052	insertion	hypothetical
slt	3,436,184	F19-10-MH12	1051	insertion	lytic transglycosylase, catalytic
deaD	3,505,771	F19-10-CH6, F19-10-8	91	deletion	DEAD / DEAH boxhelicase
	3,506,010	F19-10-MH12	90	deletion	
yjjK	3,635,555	F19-10-CH6	66	deletion	Energy-dependent translational throttle protein EttA
hypothetical	3,668,510	F19-10-MH12	1051	insertion	Unknown
hypothetical	3,675,512	F19-10-MH12	1052	insertion	Unknown
hypothetical	3,791,684	F19-10-9	1043	insertion	Unknown
hypothetical	3,793,960	F19-10-9	2275	deletion	Unknown
	3,793,964	F19-10-2	1052	insertion	
ABUW_0118	3,794,514	F19-10-MH12	1052	insertion	hypothetical
hypothetical	3,795,281	F19-10-4	1043	insertion	Unknown
hypothetical	3,796,423	F19-10-MH6	1043	insertion	Unknown
vgrG	3,801,263	F19-10-2	5624	insertion	Type VI secretion system tip protein VgrG
		F19-10-9	5771		
hypothetical	3,809,149	F19-10-MH6	12725	deletion	Unknown
comM	3,816,243	F19-10-4	20961	deletion	Competence protein ComM
5S ribosomal RNA gene	3,851,658	F19-10-2	5382	insertion	5S ribosomal RNA
			5571	deletion	
mpl	4,044,909	F19-10-MH6	1052	insertion	UDP-N-acetylmuramate:L-alanyl-gamma-D-glutamyl-meso-diaminopimelate ligase

645

INTERGENIC VARIATIONS								
Support	Position	Strains	Size	Type	Upstream		Downstream	
					Gene	Product	Gene	Product
Plasmid	12,704	F19-10-MH6	601	deletion	*ATPase gene*	ATPase	*transposase gene*	transposase
	14,346	F16-03, F19-02, F19-10-CH6, F19-10-MH6, F19-10-8	104	insertion	*ABUW_3803*	putative transposase (ISN4)	*higB-2*	Toxin HigB-2
	14,483	F15-06, F19-10-4	105	insertion				
	19,535	F19-10-8	115	deletion	*Transposition gene*	Transposition protein	*rcr2*	ISS1-like element ISVsa5 family transposase
	24,188	F19-02	154	deletion	*Transposition gene*	Transposition protein	*aacA-aphD*	Bifunctional AAC/APH
	27,244	F19-10-CH3, F19-10-CH8	29	deletion	*aacA-aphD*	Bifunctional AAC/APH	*hypothetical*	Unknown
	107,681	F19-10-4	1052	insertion	*ABUW_3838*	hypothetical	*hypothetical*	Unknown
	141,880	F19-10-CH6	6	insertion	*transposase gene*	Transposition protein	*DNA-binding ATP-dependent protease gene*	DNA-binding ATP-dependent protease
chromosome	177,139	F19-10-4	1	snp	*hvrA*	Putative DNA binding protein	*ABUW_3408*	general secretion pathway protein
	208,625	F19-10-MH12	1	snp	*ABUW_3583*	Putative outer membrane protein W	*ABUW_3582*	hypothetical
	338,079	F19-10-MH12	1	snp	*ABUW_3650*	endonuclease/exonuclease/phosphatase	*dctA*	C4-dicarboxylate transport protein
	376,760	F19-10-2, F19-10-9	1	snp	*purU*	formyl tetrahydrofolate deformylase	*tonB*	Siderophore-mediated iron transport protein
	401,066	F19-10-CH6, F19-10-8, F19-10-MH12	1	snp	*bfpD*	Putative ferric siderophore receptor protein	*tig*	trigger factor
	401,065	F19-10-MH12	4	insertion				
	457,460	F19-10-2, F19-10-CH3, F19-10-CH8, F19-10-9	2	deletion	*ilvC*	ketol-acid reductoisomerase	*ABUW_3358*	ggdef domain/ealdomain protein
	600,981	F19-10-CH3, F19-10-CH8	1	snp	*hypothetical*	Unknown	*fliC*	Flagellum assembly protein FliC
	601,008	F19-10-CH6, F19-10-8	1	snp				
	621,964	F19-10-2, F19-10-CH3, F19-10-CH8, F19-10-9	1	snp	*argJ*	glutamate N-acetyltransferase/amino-acid acetyltransferase	*nqrA*	quinolinate synthetase complex, A subunit
	998,117	F19-10-2, F19-10-CH3, F19-10-CH8, F19-10-9	1	snp	*rubA*	rubredoxin	*ABUW_2901*	activator of HSP90 ATPase
	1,234,233	F19-10-CH6, F19-10-8	1	snp	*ABUW_2700*	hypothetical	*ABUW_2689*	hypothetical
	1,249,389	F19-10-2, F19-10-9	1	snp	*ABUW_2678*	17 kDa surface antigen	*hypothetical*	Unknown
	1,402,482	F19-10-CH3, F19-10-CH8	2	deletion	*ABUW_2533*	hypothetical	*ABUW_2531*	Dihydrodipicolinate synthetase
	1,413,342	F19-10-MH12	3	deletion	*aldH*	aldehyde dehydrogenase	*yveA*	amino acid transporter
	1,570,384	F19-10-CH3, F19-10-CH8	1	snp	*cioA*	cytochrome bd ubiquinol oxidase, subunit I	*ABUW_2387*	hypothetical
	1,861,760	F19-02, F19-02	1	snp	*rnd*	ribonuclease D	*ABUW_2145*	hypothetical
	1,918,607	F19-10-2, F19-10-9	1	snp	*ABUW_0797*	lipoprotein, putative	*ABUW_2093*	GntP family transporter
	1,926,643	F19-10-2, F19-10-9	1	snp	*baoC*	short chain dehydrogenase	*ABUW_2087*	oxygenase subunit
	2,198,987	F19-10-CH3	1	snp	*aroD*	3-dehydroquinate dehydratase	*ABUW_1815*	hypothetical
	2,237,481	F19-10-MH12	1	snp	*ABUW_1773*	alpha/beta hydrolase	*fhuB*	multiphosphonate transfer protein
	2,254,764	F19-10-MH12	1	snp	*apyA*	Putative alkaline serine protease	*ABUW_1728*	hypothetical
	2,295,760	F19-10-MH12	1	snp	*ABUW_1714*	transcriptional regulator, MarR family	*moaA*	Molybdopterin molybdenum transferase
	2,390,338	F19-10-CH3	1	snp	*acoI*	Short-chain dehydrogenase	*acoR*	MTH-type transcriptional regulator AcoR
	2,488,396	F19-10-2, F19-10-9	1	snp	*tfp*	host factor Hfq	*miaA*	tRNA delta(2)-isopentenylpyrophosphate transferase
	2,623,054	F19-10-2, F19-10-9	1	snp	*csuA/B*	Fimbrial major subunit CsuA/B family protein	*ABUW_1485*	transcriptional regulator, TetR family protein
	2,645,163	F19-02, F19-02	2	deletion	*hypothetical*	Unknown	*hypothetical*	Unknown
	2,688,295	F19-10-2, F19-10-9	1	snp	*thiG*	thiazole biosynthesis protein ThiG	*hypothetical*	Unknown
	2,688,383	F19-10-MH12	1	snp				
	2,692,291	F19-10-CH6, F19-10-8	1	snp	*norR*	Anaerobic nitric oxide reductase transcription regulator NorR	*rna*	ribonuclease 2
	2,713,672	F19-10-2, F19-10-9	1	snp	*ABUW_1336*	MutT/NUDIX family protein	*hemp*	Heme transporter HemP
	2,729,458	F19-10-9	1	snp	*hbl*	Nucleine binding periplasmic protein	*yfjC*	Transcriptional regulator, LysR family
	2,754,481	F19-02, F19-02	1	snp	*map1*	methionine aminopeptidase, type I	*ompW*	OmpW family protein
	2,761,878	F19-10-2, F19-10-CH3, F19-10-CH8, F19-10-9	1	snp	*lipA1*	lipoic acid synthetase	*fldE*	acyl-CoA dehydrogenase
	2,926,509	F19-10-CH6, F19-10-8	2	deletion	*icd*	isocitrate dehydrogenase, NADP-dependent	*rluE*	Pseudouridine synthase
	3,086,114	F19-10-MH12	1	snp	*ABUW_0825*	lytic transglycosylase, catalytic	*htpX*	heat shock protein HtpX
	3,386,381	F19-10-MH12	5	complex	*16S ribosomal RNA gene*	16S ribosomal RNA	*ABUW_0507*	hypothetical
	3,400,287	F19-10-MH12	1	snp	*ABUW_0504*	Ser/Thr protein phosphatase family protein	*pld*	Phospholipase D
	3,423,746	F19-10-CH6, F19-10-8	1	snp	*ABUW_0468*	hypothetical	*mdh*	malate dehydrogenase
	3,583,322	F19-10-CH6, F19-10-8, F19-10-MH12	3	deletion	*ABUW_0307*	hypothetical	*bfr1*	bacterioferritin
	3,681,310	F19-10-CH6, F19-10-8	1	snp	*ABUW_0263*	cation efflux system protein	*czcN*	Protein S-isoprenylcysteine methyltransferase
	3,758,205	F19-10-2, F19-10-9	1	snp	*ftsA*	cell division protein FtsA	*ftsQ*	cell division protein FtsQ
	3,954,309	F19-10-MH12	1	snp	*hypothetical*	Unknown	*hypothetical*	Unknown
	4,023,648	F19-10-2, F19-10-9	1	snp	*ABUW_3845*	putative flavoprotein	*5S ribosomal RNA gene*	5S ribosomal RNA
	17,536	F19-02	65	deletion	*tyrS*	tyrosyl-tRNA synthetase	*16S ribosomal RNA gene*	16S ribosomal RNA
	17,546	F19-10-MH6	57	deletion				
	17,564	F19-10-CH3, F19-10-4, F19-10-CH8	48	deletion				
	17,589	F19-10-MH12	20	insertion				
	17,591	F15-01A, F19-10-2	9	deletion				
	17,597	F15-01B, F15-02, F18-02, F19-10-CH6	9	insertion				
	17,830	F19-10-4	5747	insertion				
	17,830	F19-10-4	5643	deletion				
	17,881	F19-10-MH6	5686	insertion				
	17,881	F19-10-MH6	5555	deletion				
	18,059	F19-10-2, F19-10-CH3, F19-10-CH8	5518	insertion				
	18,059	F19-10-2, F19-10-CH3, F19-10-CH8	5411	deletion				
	18,159	F19-10-9	5418	insertion				
	18,159	F19-10-9	5350	deletion				
	123,747	F19-10-MH12	1043	insertion	*ABUW_0594*	AAA ATPase	*blaOXA-133*	beta-lactamase OXA-23
			2868	deletion				
	125,862	F19-10-CH3, F19-10-CH8	2402	deletion	*transposase gene*	Transposition protein	*ABUW_3838*	hypothetical
	127,983	F19-10-9	8448	deletion	*ABUW_3838*	hypothetical	*comM*	Competence protein ComM
	176,749	F19-10-MH12	1052	insertion	*yomA*	Nucleotidase superfamily protein	*hvrA*	Putative DNA binding protein
	177,266	F19-10-4	371	deletion	*hvrA*	Putative DNA binding protein	*ABUW_3408*	general secretion pathway protein
	203,672	F19-10-4, F19-10-MH6	1193	insertion	*ABUW_3583*	Putative outer membrane protein W	*ABUW_3582*	hypothetical
	406,563	F19-10-MH12	1051	insertion	*ABUW_3338*	hypothetical	*fumA*	fumarate hydratase
	584,465	F19-10-MH12	1471	insertion	*vacJ*	VacJ family lipoprotein	*16S ribosomal RNA*	
	615,869	F19-10-MH12	1051	insertion	*ABUW_3225*	hypothetical	*pcoA*	copper resistance protein A
	623,803	F19-10-CH6	7	insertion	*tRNA-Pro*	adenosine deaminase	*add2*	adenosine deaminase
	623,833	F19-02	7	deletion				
	623,899	F19-02	7	insertion				
	623,906	F19-10-4	67	deletion				
	623,916	F19-02	32	insertion				
	623,921	F19-10-9	14	insertion				
	623,923	F19-10-MH12	25	deletion				
	623,924	F19-10-2	7	insertion				
	623,941	F15-05	7	insertion				
	623,943	F19-10-8	25	insertion				
	844,958	F19-10-MH12	1043	insertion	*ABUW_1281*	hypothetical	*hypothetical*	
	891,183	F19-10-MH12	1052	insertion	*ABUW_2882*	hypothetical	*putative type I restriction enzyme HsdM gene*	putative type I restriction enzyme HsdM protein
	934,606	F19-10-9	1052	insertion	*fbp*	Peptidyl-prolyl cis-trans isomerase	*pgaB*	Biofilm PGA synthesis lipoprotein PgaB
	934,615	F19-10-2	1052	insertion				
	998,915	F19-10-9	33	insertion	*rubA*	rubredoxin	*ABUW_2901*	activator of HSP90 ATPase
	998,949	F19-10-9	33	deletion				
	999,070	F19-10-2	16550	deletion				
	1,084,606	F19-10-MH12	12190	deletion	*ABUW_3415*	transcriptional regulator, LysR family	*exuT*	Hexuronate transporter
	1,096,030	F19-10-4, F19-10-MH6	1052	insertion	*pcaF1*	beta-ketoadipyl CoA thiolase	*hypothetical*	
	1,112,244	F19-10-9	1051	insertion	*astA2*	arginine N-succinyltransferase	*cycA*	D-alanine/D-serine/glycine permease
	1,112,251	F19-10-2	1051	insertion				
	1,234,327	F19-10-8	49	deletion	*ABUW_2700*	hypothetical	*ABUW_2689*	hypothetical
	1,234,376	F19-10-8	49	insertion				
	1,234,427	F19-10-8	7094	deletion				
	1,247,386	F19-10-MH12	1051	insertion	*ABUW_2681*	hypothetical	*ABUW_2679*	hypothetical
	1,249,691	F19-10-MH12	1052	insertion	*ABUW_2678*	17 kDa surface antigen	*hypothetical*	
	1,250,046	F19-02, F19-10-8	44075	deletion				
	1,313,077	F19-10-CH3	13475	deletion	*ABUW_2633*	transcriptional regulator	*ybiF*	inner membrane transport protein YbiF
	1,313,126	F19-10-CH8	13624	deletion				
	1,347,431	F19-10-MH12	53816	deletion	*ABUW_2585*	hypothetical	*ybdR*	Glutathione-dependent formaldehyde dehydrogenase
	1,400,666	F19-10-2	1043	insertion	*ABUW_2556*	hypothetical	*soxR*	redox-sensitive transcriptional activator SoxR
	1,403,575	F19-10-MH12	1193	insertion	*dapA*	Dihydrodipicolinate synthetase	*yejM*	Permease of the drug/metabolite transporter (DMT) superfamily
	1,517,021	F19-10-MH12	3610	deletion	*ABUW_2437*	heme oxygenase-like protein	*katE*	catalase
	1,577,977	F19-10-MH6	1052	insertion	*ABUW_2383*	signal peptide protein	*tauA*	taurine ABC transporter, periplasmic binding protein
	1,605,359	F19-10-MH12	130	deletion	*aspQ*	L-asparaginase 2	*dctA*	Sodium-dicarboxylate symporter
	1,605,489	F19-10-MH12	1043	insertion				
	1,643,704	F19-10-8	1316	deletion	*ABUW_2319*	putative membrane protein	*transposase gene*	transposase of ISAba34
	1,643,707	F19-10-CH6	1315	insertion				
	1,688,794	F19-10-2, F19-10-9	1052	insertion	*ABUW_2275*	transcriptional regulator, TetR family	*ABUW_2274*	cupin family protein
	1,906,575	F19-10-MH12	1052	insertion	*aspA*	fumarate lyase	*ABUW_2103*	hypothetical
	1,918,699	F19-10-2, F19-10-9	1051	insertion	*ABUW_0797*	putative lipoprotein	*ABUW_2093*	GntP family transporter
	1,918,693	F19-10-MH12	1053					
	1,918,842	F19-10-4	1052					
	1,921,532	F19-10-MH12	1051	insertion	*bdhA*	3-hydroxybutyrate dehydrogenase	*xylS*	transcriptional regulator, AraC family
	1,963,700	F19-10-MH12	1052	insertion	*ABUW_2053*	hypothetical	*hypothetical*	
	2,019,204	F19-10-MH12	1052	insertion	*hypothetical*	Unknown	*hypothetical*	Unknown
	2,110,370	F19-10-MH12	1052	insertion	*ABUW_1885*	hypothetical	*katE*	catalase
	2,117,104	F19-10-MH12	1052	insertion	*ABUW_0735*	NADPH quinone oxidoreductase	*ABUW_0184*	Nat/solute symporter
	2,126,962	F19-10-MH12	1052	insertion	*hypothetical*	Unknown	*atiN*	2-ketoglutarate semialdehyde dehydrogenase
	2,217,414	F19-10-4, F19-10-MH6	1193	insertion				

	2,217,422	F19-10-2, F19-10-CH3, F19-10-CH8, F19-10-9	1192	insertion	ABUW_1800	ferrichrome-iron receptor	ABUW_1799	sugar kinase, ribokinase family
	2,361,629	F19-10-CH8	43132	deletion	ABUW_2322	phage integrase	ABUW_1693	heme oxygenase-like protein
	2,361,646	F19-10-CH6	23	insertion				
	2,364,187	F19-10-MH12	1052	insertion	ABUW_1692	transcriptional regulator, TetR family	ABUW_1691	PepSY-associated TM helix domain-containing protein
	2,398,886	F19-10-MH12	1052	insertion	ABUW_1665	hypothetical	ABUW_1664	RDD domain-containing protein
	2,407,941	F19-10-MH6	1044	insertion	ABUW_1655	TonB-dependent siderophore receptor	ABUW_1654	acetyltransferase, gnat family
	2,410,238	F19-10-MH12	1041	insertion	ABUW_1651	hypothetical	ABUW_1645	hypothetical
	2,421,900	F15-06	1213	insertion	ABUW_1671	hca operon transcriptional activator	transposase gene	transposase of ISAba34
		F19-10-CH3, F19-10-CH8	1211					
	2,568,364	F19-10-CH6	1028	insertion	ppgA	outer membrane protein	ABUW_1336	Putative phosphoenolpyruvate synthase regulatory protein
	2,568,366	F19-10-4, F19-10-MH6	270	deletion				
	2,568,366	F15-01B, F15-02, F19-10-MH12	1052	insertion				
		F19-10-8	1039					
	2,568,371	F15-06, F19-10-2, F19-10-9	1052	insertion				
		F19-10-CH3, F19-10-CH8	1042					
	2,568,468	F19-10-2, F19-10-9	86	deletion				
	2,622,988	F15-01A	1052	insertion	csuA/B	Fimbrial major subunit CsuA/B family protein	ABUW_1486	transcriptional regulator, TetR family protein
	2,622,993	F19-10-4	1052	insertion				
	2,623,327	F19-10-MH12	113	deletion				
	2,637,723	F19-10-MH12	1052	insertion	gabP	Gamma-aminobutyrate transport protein	mmsA2	methylmalonate-semialdehyde dehydrogenase
	2,641,889	F19-10-4	1052	insertion	ABUW_1482	transcriptional regulator, LysR family	hypothetical	
	2,698,697	F19-10-4	1052	insertion	pepG	aminoacyl-histidine dipeptidase	ABUW_1367	Type III secretion protein
	2,930,186	F19-10-9	1192	insertion	idh	isocitrate dehydrogenase, NADP-dependent	ABUW_1073	peptidase M61
	2,930,194	F19-10-2	1193	insertion				
	2,954,212	F19-10-4, F19-10-MH6	1052	insertion	ABUW_1031	hypothetical	gap	glyceraldehyde-3-phosphate dehydrogenase
	3,064,900	F19-10-9	1052	insertion	yde,P	Putative oxidoreductase molybdopterin	aiiA	Glyoxalase
	3,068,431	F19-10-4	1052	insertion	dnpA	NAD(P)H nitroreductase	hypothetical	
	3,078,688	F19-10-MH12	1052	insertion	ABUW_0832	non-ribosomal peptide synthetase	ABUW_0831	hypothetical
	3,078,823	F19-10-MH12	1052	insertion				
	3,137,764	F19-10-MH12	1052	insertion	hypothetical		nhaT	putative Na+/H+ antiporter
	3,312,870	F19-10-MH12	1052	insertion	gatD	Putative methyltransferase	yfiA	Putative hemolysin III (HLY-III)
	3,396,934	F19-10-MH12	11545	deletion	16S ribosomal RNA		ABUW_0507	hypothetical
	3,542,749	F19-10-MH12	1043	insertion	gdh	glutamate dehydrogenase	mmuP	Putative APC family, S-methylmethionine transporter (MmuP)
	3,543,223	F19-10-MH12	473	deletion				
	3,791,019	F19-10-4	1052	insertion	hypothetical		hypothetical	
	3,792,411	F19-10-4	1052	insertion	hypothetical		ABUW_0121	hypothetical
	3,861,633	F19-10-4	5683	insertion	ABUW_3710	putative acetyltransferase	23S ribosomal RNA	
		F19-10-MH6	5666					
	3,861,670	F19-10-CH3	5520	insertion				
	3,861,670	F19-10-CH3	5658	deletion				
	3,861,671	F19-10-CH8	5520	insertion				
		F19-10-9	5498					
	3,861,671	F19-10-CH8	5658	deletion				
		F19-10-9	5608					
	3,867,181	F19-10-9	5526	deletion	16S ribosomal RNA		ABUW_3716	transcriptional regulator domain-containing protein
	3,867,230	F19-10-2	5507	deletion				
		F19-10-CH3	5507					
		F19-10-CH8	5568					
	3,916,216	F19-10-MH12	1052	insertion	ABUW_3773	acyl-CoA synthetase/AMP-acid ligase	sdiR	Probable transcriptional activator of quorum sensing autoinducer synthesis transcription regulator protein
	3,916,561	F19-10-MH12	1052	insertion				
	3,917,908	F19-10-4	1052	insertion	sdiR	Probable transcriptional activator of quorum sensing autoinducer synthesis transcription regulator protein	ABUW_3775	hypothetical
	3,917,917	F19-10-MH12	1052	insertion				
	3,951,294	F19-10-MH12	1052	insertion	fabB	3-oxoacyl-[acyl-carrier-protein] synthase 1	hypothetical	
	4,023,651	F19-10-2, F19-10-CH3, F19-10-CH8	5389	insertion	ABUW_3863	putative flavoprotein	23S ribosomal RNA	
		F19-10-9	5379					
	4,041,600	F19-10-MH12	324	deletion	mtlB	putative transglycosylase	purK	phosphoribosylaminoimidazole carboxylase, ATPase subunit
	4,041,924	F19-10-MH12	1043	insertion				
	4,061,787	F19-10-4	10761	deletion	rpmH	ribosomal protein L34	dnaA	chromosomal replication initiator protein DnaA
		F19-10-MH6	10762					
	4,061,788	F19-02	2339	deletion				
		F19-10-CH6	10648					
		F19-10-8	10465					

647

648 **TABLE S4**. Bacterial strains and primers used in this study.

Strains		
Strain name	Description/phenotype	Reference
40288	*A. baumannii* veterinary clinical strain 40288; carbapenem resistant	(26)
DSM30011	*A. baumannii* environmental strain	(33)
F14-11	*A. baumannii* veterinary clinical strain isolated in November 2014	This study
F15-01A	*A. baumannii* veterinary clinical strain isolated in January 2015	This study
F15-01B	*A. baumannii* veterinary clinical strain isolated in January 2015	This study
F15-02	*A. baumannii* veterinary clinical strain isolated in February 2015	This study
F15-06	*A. baumannii* veterinary clinical strain isolated in June 2015	This study
F16-05	*A. baumannii* veterinary clinical strain isolated in May 2016	This study
F18-02	*A. baumannii* veterinary clinical strain isolated in February 2018	This study
F19-02	*A. baumannii* veterinary clinical strain isolated in February 2019	This study
F19-10-2	*A. baumannii* supplementary strain isolated in October 2019 isolated on LB-agar	This study
F19-10-4	*A. baumannii* supplementary strain isolated in October 2019 isolated on LB-agar	This study
F19-10-8	*A. baumannii* supplementary strain isolated in October 2019 isolated on LB-agar	This study
F19-10-9	*A. baumannii* supplementary strain isolated in October 2019 isolated on LB-agar	This study
F19-10-MH6	*A. baumannii* supplementary strain isolated in October 2019 isolated on Mueller-Hinton-agar	This study
F19-10-MH12	*A. baumannii* supplementary strain isolated in October 2019 isolated on Mueller-Hinton-agar	This study
F19-10-CH3	*A. baumannii* supplementary strain isolated in October 2019 isolated on CHROMagar	This study

F19-10-CH6	*A. baumannii* supplementary strain isolated in October 2019 isolated on CHROMagar	This study
F19-10-CH8	*A. baumannii* supplementary strain isolated in October 2019 isolated on CHROMagar	This study
Fluorescent derivatives	*att*Tn*7*::*sf-gfp, aac*	This study
F14-11 Δ*higA-higB*::*sacB-aac4*	F14-11 derivative with replacement of *higAB* toxin-antitoxin genes with *sacB-aac4* cassette	This study
F14-11Δ*prp*	F14-11 derivative deleted for the *prp* operon	This study
F14-11Δ*pilA::kan*	F14-11 derivative with an insertion of a kanamycin resistance cassette in the *pilA* gene	This study
F14-11 p-	F14-11 plasmid-less derivative	This study
F14-11Δ*pmrB*	F14-11 derivative deleted for *pmrB*	This study
F14-11 PmrB(P170T)	F14-11 derivative encoding the PmrB(P170T) substitution	This study
A118	*A. baumannii* strain A118 wild-type	(70)
M2	*A. nosocomialis* strain M2 wild-type	(71)
AB5075	*A. baumannii* model strain AB5075 wild-type	(72)
17978	*A. baumannii* model strain ATCC 17978 wild-type	(73)

Primers			
Genetic construct	Name	Primer Sequence 5’ to 3’	Template; Annealing site
Chromosomal modifications using overlap extension PCR			
Δ*higA-higB*::*sacB-aac4*	mlo-132	tgcgacttaacggctgatatacgc	F14-11 genomic DNA; 2kb upstream of the *higB-2* gene
	mlo-133	**ggaacttcgaagcagctccagcctacacaatc**cataggtttaagtacgtcaatggcg	F14-11 genomic DNA; Chimeric, **apdater**-3’ and upstream *higB-2*

	mlo-186	**gattgtgtaggctggagctgcttcgaagttccatc**acccatcacatatacctgccgttcac	pMHL-10 (26); upstream of *sacB* with an **adapter** sequence
	Apra_Rev3	**gccatggtccatatgaatatcctccttagtt**ctcatgagctcagccaatcgactgg	pMHL-10 (26); downstream *aacC4* gene with an **adapter** sequence
	mlo-134	**aactaaggaggatattcatatggaccatggc** tgctgcacgcttacatattagcgcg	F14-11 genomic DNA; Chimeric **adapter**and 5' of *higA-2* gene
	mlo-125	cttcagttcacgcatcaagcttgt	F14-11 genomic DNA; 2kb downstream of *higA-2* gene
PmrB(P170T) and Δ*pmrB*	lb-16	tgtgattggtggtgcagcgg	F14-11/F15-01A genomic DNA; 2kb upstream the *pmrB* SNP encoding the PmrB(P170T) substitution
	lb-17	ggtacggcaacagcggtttc	F14-11/F15-01A genomic DNA; 2kb downstream the *pmrB* SNP encoding the PmrB(P170T) substitution
	lb-23	**cagctccagcctacacaatc**ctacgaacacctgtgactgc	F14-11 genomic DNA; *pmrB* gene with an **adapter** sequence
	lb-28	**aggatattcatatggaccatggc**gaggtgccccaaatcagtcg	F14-11 genomic DNA; *pmrB* gene with an **adapter** sequence
	lb-29	**gattgtgtaggctggagctg**gaggtgccccaaatcagtcg	F14-11 genomic DNA; *pmrB* gene with an **adapter** sequence
Fluorescent derivatives	lb-1	cctgtttgatggtggttgtgttg	pASG-1 (74); upstream *sf-gfp* gene
	lb-2	atactggcgacttctctgaacg	pASG-1 (74); downstream *aac* gene
	lb-3	gttcatccatgccatgtgtaatcc	F14-11 genomic DNA; 2-kb upstream *att*Tn7 site
	lb-4	**gtcaacacaaccaccatcaaacagg**ctgatttattaagcccgatatgc	F14-11 genomic DNA; *att*Tn7 site with an **adapter** sequence
	lb-5	gggattacacatggcatggatgaac**ttattaaagcaggtgatgcc**	F14-11 genomic DNA; *att*Tn7 site with an **adapter** sequence

	oac-6	tggtaatggagcaacagtcg	F14-11 genomic DNA; 2-kb downstream *att*Tn7 site
Δ*prp*	lb-6	cgtaatgcggcccaacgtag	F14-11 genomic DNA; 2-kb upstream *prp* operon
	lb-7	**aggatattcatatggaccatggc**cgatattcctttaacggcgcg	F14-11 genomic DNA; *prpD* with an **adapter** sequence
	lb-8	**cagctccagcctacacaatc**atcagctgcttgtgctgctg	14-11 genomic DNA; *prpA* with an **adapter** sequence
	lb-9	caccgtgagcacttcactgc	F14-11 genomic DNA; 2-kb downstream *prp* operon
Δ*pilA::kan*	asg-151	tcagaatgcggcttggag	F14-11 genomic DNA; 2-kb upstream *pilA* gene
	asg-152	tgccaaagttatttgctg	F14-11 genomic DNA; 2-kb downstream *pilA* gene
	lb-21	**ccttcttcacgaggca**gcttgtccagtaggaacacc	F14-11 genomic DNA; *pilA* gene with an **adapter** sequence
	lb-22	**gaacacttgaggcgcag**gctgctacattagagcgacc	F14-11 genomic DNA; *pilA* gene with an **adapter** sequence
	Kan-R	**tgcctcgtgaagaagg**	KanR gene cassette ; downstream the *kanR* gene
	Kan-F	**ctgcgcctcaagtgttc**	KanR gene cassette ; upstream the *kanR* gene

649

650 **References**

651 1. Nocera FP, Attili A-R, De Martino L. 2021. Acinetobacter baumannii: Its Clinical
652 Significance in Human and Veterinary Medicine. 2. Pathogens 10:127.
653 2. van der Kolk JH, Endimiani A, Graubner C, Gerber V, Perreten V. 2019.
654 Acinetobacter in veterinary medicine, with an emphasis on Acinetobacter baumannii.
655 J Glob Antimicrob Resist 16:59–71.
656 3. Sun R, Song P, Walline J, Wang H, Xu Y, Zhu H, Yu X, Xu J. 2020. Morbidity
657 and mortality risk factors in emergency department patients with Acinetobacter
658 baumannii bacteremia. World J Emerg Med 11:164–168.
659 4. Iacono M, Villa L, Fortini D, Bordoni R, Imperi F, Bonnal RJP, Sicheritz-Ponten
660 T, De Bellis G, Visca P, Cassone A, Carattoli A. 2008. Whole-Genome Pyrosequencing
661 of an Epidemic Multidrug-Resistant Acinetobacter baumannii Strain Belonging to the
662 European Clone II Group †. ANTIMICROBIAL AGENTS AND CHEMOTHERAPY
663 52:2616–2625.
664 5. Tacconelli E. 2018. Discovery, research, and development of new antibiotics:
665 the WHO priority list of antibiotic-resistant bacteria and tuberculosis. The Lancet
666 Infectious Diseases 18:318–327.
667 6. Lupo A, Châtre P, Ponsin C, Saras E, Boulouis H-J, Keck N, Haenni M, Madec
668 J-Y. 2016. Clonal Spread of Acinetobacter baumannii Sequence Type 25 Carrying
669 blaOXA-23 in Companion Animals in France. Antimicrobial Agents and Chemotherapy
670 61:10.1128/aac.01881-16.
671 7. Maragakis LL, Perl TM. 2008. Acinetobacter baumannii: epidemiology,
672 antimicrobial resistance, and treatment options. Clin Infect Dis 46:1254–1263.
673 8. Bordenave Sylvain, Goñi-Urriza María Soledad, Caumette Pierre, Duran
674 Robert. 2007. Effects of Heavy Fuel Oil on the Bacterial Community Structure of a
675 Pristine Microbial Mat. Applied and Environmental Microbiology 73:6089–6097.
676 9. Sarma PM, Bhattacharya D, Krishnan S, Lal B. 2004. Assessment of intra-
677 species diversity among strains of Acinetobacter baumannii isolated from sites
678 contaminated with petroleum hydrocarbons. Can J Microbiol 50:405–414.
679 10. Eveillard M, Kempf M, Belmonte O, Pailhoriès H, Joly-Guillou M-L. 2013.
680 Reservoirs of Acinetobacter baumannii outside the hospital and potential involvement
681 in emerging human community-acquired infections. Int J Infect Dis 17:e802-805.

682 11. Wilharm G, Skiebe E, Łopińska A, Higgins PG, Weber K, Schaudinn C,
683 Neugebauer C, Görlitz K, Meimers G, Rizova Y, Blaschke U, Heider C, Cuny C,
684 Drewes S, Heuser E, Jeske K, Jacob J, Ulrich RG, Bochenski M, Kasprzak M, Burda
685 E, Ciepliński M, Kaługa I, Jankowiak Ł, Aguirre JI, López-García A, Höfle U, Jagiello
686 Z, Tobółka M, Janic B, Zieliński P, Kamiński M, Frisch J, Siekiera J, Wendel AF,
687 Brauner P, Jäckel U, Kaatz M, Müller S, Lübke-Becker A, Wieler LH, Wachsmann J
688 von, Thrukonda L, Helal M, Epping L, Wolf SA, Semmler T, Jerzak L. 2024. On the
689 ecology of Acinetobacter baumannii – jet stream rider and opportunist by nature.
690 bioRxiv https://doi.org/10.1101/2024.01.15.572815.
691 12. Hawkey J, Ascher DB, Judd LM, Wick RR, Kostoulias X, Cleland H, Spelman
692 DW, Padiglione A, Peleg AY, Holt KE. 2018. Evolution of carbapenem resistance in
693 Acinetobacter baumannii during a prolonged infection. Microb Genom 4:e000165.
694 13. Kim M, Park J, Park W. 2021. Genomic and phenotypic analyses of multidrug-
695 resistant Acinetobacter baumannii NCCP 16007 isolated from a patient with a urinary
696 tract infection. Virulence 12:150–164.
697 14. Zhang J, Xie J, Li H, Wang Z, Yin Y, Wang S, Chen H, Wang Q, Wang H. 2022.
698 Genomic and Phenotypic Evolution of Tigecycline-Resistant Acinetobacter baumannii
699 in Critically Ill Patients. Microbiol Spectr 10:e0159321.
700 15. Wright MS, Iovleva A, Jacobs MR, Bonomo RA, Adams MD. 2016. Genome
701 dynamics of multidrug-resistant Acinetobacter baumannii during infection and
702 treatment. Genome Medicine 8:26.
703 16. Li H, Zhang J, Wang Z, Yin Y, Gao H, Wang R, Jin L, Wang Q, Zhao C, Wang
704 Z, Wang H. 2021. Evolution of Acinetobacter baumannii in Clinical Bacteremia
705 Patients. Infect Drug Resist 14:3553–3562.
706 17. Penesyan A, Nagy SS, Kjelleberg S, Gillings MR, Paulsen IT. 2019. Rapid
707 microevolution of biofilm cells in response to antibiotics. npj Biofilms Microbiomes 5:1–
708 14.
709 18. Lila ASA, Rajab AAH, Abdallah MH, Rizvi SMD, Moin A, Khafagy E-S, Tabrez
710 S, Hegazy WAH. 2023. Biofilm Lifestyle in Recurrent Urinary Tract Infections. 1. Life
711 13:148.
712 19. Venanzio GD, Moon KH, Weber BS, Lopez J, Ly PM, Potter RF, Dantas G,
713 Feldman MF. 2019. Multidrug-resistant plasmids repress chromosomally encoded
714 T6SS to enable their dissemination. PNAS 116:1378–1383.

715 20. Venanzio GD, Flores-Mireles AL, Calix JJ, Haurat MF, Scott NE, Palmer LD,
716 Potter RF, Hibbing ME, Friedman L, Wang B, Dantas G, Skaar EP, Hultgren SJ,
717 Feldman MF. 2019. Urinary tract colonization is enhanced by a plasmid that regulates
718 uropathogenic Acinetobacter baumannii chromosomal genes. Nature
719 Communications 10:2763.
720 21. Benomar S, Di Venanzio G, Feldman MF. 2021. Plasmid-encoded H-NS
721 controls extracellular matrix composition in a modern Acinetobacter baumannii urinary
722 isolate. J Bacteriol JB0027721.
723 22. Kopecny L, Palm CA, Drobatz KJ, Balsa IM, Culp WTN. 2019. Risk factors for
724 positive urine cultures in cats with subcutaneous ureteral bypass and ureteral stents
725 (2010-2016). J Vet Intern Med 33:178–183.
726 23. Moustafa AM, Planet PJ. 2020. WhatsGNU: a tool for identifying proteomic
727 novelty. Genome Biol 21:58.
728 24. Hamidian M, Hall RM. 2016. The resistance gene complement of D4, a multiply
729 antibiotic-resistant ST25 Acinetobacter baumannii isolate, resides in two genomic
730 islands and a plasmid. Journal of Antimicrobial Chemotherapy 71:1730–1732.
731 25. Lupo A, Valot B, Saras E, Drapeau A, Robert M, Bour M, Haenni M, Plésiat P,
732 Madec J-Y, Potron A. 2023. Multiple host colonization and differential expansion of
733 multidrug-resistant ST25-Acinetobacter baumannii clades. Sci Rep 13:21854.
734 26. Godeux A-S, Svedholm E, Barreto S, Potron A, Venner S, Charpentier X,
735 Laaberki M-H. 2022. Interbacterial Transfer of Carbapenem Resistance and Large
736 Antibiotic Resistance Islands by Natural Transformation in Pathogenic Acinetobacter.
737 mBio 13:e02631-21.
738 27. Rafei R, Koong J, Osman M, Al Atrouni A, Hamze M, Hamidian M. 2022.
739 Analysis of pCI107 a large plasmid carried by an ST25 Acinetobacter baumannii strain
740 reveals a complex evolutionary history and links to multiple antibiotic resistance and
741 metabolic pathways. FEMS Microbes 3:xtac027.
742 28. Tamadonfar KO, Di Venanzio G, Pinkner JS, Dodson KW, Kalas V, Zimmerman
743 MI, Bazan Villicana J, Bowman GR, Feldman MF, Hultgren SJ. 2023. Structure–
744 function correlates of fibrinogen binding by Acinetobacter adhesins critical in catheter-
745 associated urinary tract infections. Proceedings of the National Academy of Sciences
746 120:e2212694120.

747 29. Pakharukova N, Tuittila M, Paavilainen S, Malmi H, Parilova O, Teneberg S,
748 Knight SD, Zavialov AV. 2018. Structural basis for Acinetobacter baumannii biofilm
749 formation. PNAS 115:5558–5563.
750 30. Choi AHK, Slamti L, Avci FY, Pier GB, Maira-Litrán T. 2009. The pgaABCD
751 locus of Acinetobacter baumannii encodes the production of poly-beta-1-6-N-
752 acetylglucosamine, which is critical for biofilm formation. J Bacteriol 191:5953–5963.
753 31. Loehfelm TW, Luke NR, Campagnari AA. 2008. Identification and
754 characterization of an Acinetobacter baumannii biofilm-associated protein. J Bacteriol
755 190:1036–1044.
756 32. Sahu PK, Iyer PS, Barage SH, Sonawane KD, Chopade BA. 2014.
757 Characterization of the *algC* Gene Expression Pattern in the Multidrug Resistant
758 *Acinetobacter baumannii* AIIMS 7 and Correlation with Biofilm Development on Abiotic
759 Surface. The Scientific World Journal 2014:1–14.
760 33. Repizo GD, Gagné S, Foucault-Grunenwald M-L, Borges V, Charpentier X,
761 Limansky AS, Gomes JP, Viale AM, Salcedo SP. 2015. Differential Role of the T6SS
762 in Acinetobacter baumannii Virulence. PLoS One 10:e0138265.
763 34. Pournaras S, Poulou A, Dafopoulou K, Chabane YN, Kristo I, Makris D,
764 Hardouin J, Cosette P, Tsakris A, Dé E. 2014. Growth Retardation, Reduced
765 Invasiveness, and Impaired Colistin-Mediated Cell Death Associated with Colistin
766 Resistance Development in Acinetobacter baumannii. Antimicrobial Agents and
767 Chemotherapy 58:828–832.
768 35. Kim Y, Xu W, Barrs V, Beatty J, Kenéz Á. 2022. In-depth characterisation of the
769 urine metabolome in cats with and without urinary tract diseases. Metabolomics 18:19.
770 36. Bouatra S, Aziat F, Mandal R, Guo AC, Wilson MR, Knox C, Bjorndahl TC,
771 Krishnamurthy R, Saleem F, Liu P, Dame ZT, Poelzer J, Huynh J, Yallou FS,
772 Psychogios N, Dong E, Bogumil R, Roehring C, Wishart DS. 2013. The Human Urine
773 Metabolome. PLOS ONE 8:e73076.
774 37. Jørgensen CM, Hammer K, Jensen PR, Martinussen J. 2004. Expression of the
775 pyrG gene determines the pool sizes of CTP and dCTP in Lactococcus lactis. Eur J
776 Biochem 271:2438–2445.
777 38. Alteri CJ, Smith SN, Mobley HLT. 2009. Fitness of Escherichia coli during
778 Urinary Tract Infection Requires Gluconeogenesis and the TCA Cycle. PLOS
779 Pathogens 5:e1000448.

780 39. EFSA Panel on Additives and Products or Substances used in Animal Feed
781 (FEEDAP). 2014. Scientific Opinion on the safety and efficacy of malic acid and a
782 mixture of sodium and calcium malate when used as technological additives for all
783 animal species. EFSA Journal 12:3563.
784 40. Cremin P, Kasim-Karakas S, Waterhouse AL. 2001. LC/ES-MS detection of
785 hydroxycinnamates in human plasma and urine. J Agric Food Chem 49:1747–1750.
786 41. Li T, Luo D, Ning N, Liu X, Chen F, Zhang L, Bao C, Li Z, Li D, Gu H, Qu F,
787 Yang X, Huang Y, Li B, Wang H. 2023. Acinetobacter baumannii adaptation to the host
788 pH microenvironment is mediated by allelic variation in a single residue of BauA
789 protein. PNAS Nexus 2:pgad079.
790 42. Morris EM, McGrath AP, Brejda J, Jewell DE. 2023. Relative supersaturation
791 values distinguish between feline urinary and non-urinary foods and align with
792 expected urine analytes contributions to uroliths. Front Vet Sci 10:1167840.
793 43. Good BH, McDonald MJ, Barrick JE, Lenski RE, Desai MM. 2017. The dynamics
794 of molecular evolution over 60,000 generations. Nature 551:45–50.
795 44. Schneider D, Lenski RE. 2004. Dynamics of insertion sequence elements
796 during experimental evolution of bacteria. Res Microbiol 155:319–327.
797 45. Sastre-Dominguez J, DelaFuente J, Toribio-Celestino L, Herencias C,
798 Herrador-Gómez P, Costas C, Hernández-García M, Cantón R, Rodríguez-Beltrán J,
799 Santos-Lopez A, Millan AS. 2024. Plasmid-encoded insertion sequences promote
800 rapid adaptation in clinical enterobacteria. bioRxiv
801 https://doi.org/10.1101/2024.03.01.582297.
802 46. Snitkin ES, Zelazny AM, Gupta J, NISC Comparative Sequencing Program,
803 Palmore TN, Murray PR, Segre JA. 2013. Genomic insights into the fate of colistin
804 resistance and Acinetobacter baumannii during patient treatment. Genome Res
805 23:1155–1162.
806 47. Hevia A, Delgado S, Sánchez B, Margolles A. 2015. Molecular Players Involved
807 in the Interaction Between Beneficial Bacteria and the Immune System. Frontiers in
808 Microbiology 6.
809 48. Kalu M, Tan K, Algorri M, Jorth P, Wong-Beringer A. 2022. In-Human Multiyear
810 Evolution of Carbapenem-Resistant Klebsiella pneumoniae Causing Chronic
811 Colonization and Intermittent Urinary Tract Infections: A Case Study. mSphere
812 7:e0019022.

813 49. Yamada N, Kamoshida G, Shiraishi T, Yamaguchi D, Matsuoka M, Yamauchi
814 R, Kanda N, Kamioka R, Takemoto N, Morita Y, Fujimuro M, Yokota S-I, Yahiro K.
815 2024. PmrAB, the two-component system of Acinetobacter baumannii, controls the
816 phosphoethanolamine modification of lipooligosaccharide in response to metal ions. J
817 Bacteriol e0043523.
818 50. Chaguza C, Senghore M, Bojang E, Gladstone RA, Lo SW, Tientcheu P-E,
819 Bancroft RE, Worwui A, Foster-Nyarko E, Ceesay F, Okoi C, McGee L, Klugman KP,
820 Breiman RF, Barer MR, Adegbola RA, Antonio M, Bentley SD, Kwambana-Adams BA.
821 2020. Within-host microevolution of Streptococcus pneumoniae is rapid and adaptive
822 during natural colonisation. Nat Commun 11:3442.
823 51. Gabrielaite M, Johansen HK, Molin S, Nielsen FC, Marvig RL. Gene Loss and
824 Acquisition in Lineages of Pseudomonas aeruginosa Evolving in Cystic Fibrosis
825 Patient Airways. mBio 11:e02359-20.
826 52. Barker CR, Painset A, Swift C, Jenkins C, Godbole G, Maiden MCJ, Dallman
827 TJ. 2020. Microevolution of Campylobacter jejuni during long-term infection in an
828 immunocompromised host. Sci Rep 10:10109.
829 53. Ley SD, de Vos M, Van Rie A, Warren RM. 2019. Deciphering Within-Host
830 Microevolution of Mycobacterium tuberculosis through Whole-Genome Sequencing:
831 the Phenotypic Impact and Way Forward. Microbiology and Molecular Biology Reviews
832 83:10.1128/mmbr.00062-18.
833 54. Lan F, Demaree B, Ahmed N, Abate AR. 2017. Single-cell genome sequencing
834 at ultra-high-throughput with microfluidic droplet barcoding. Nat Biotechnol 35:640–
835 646.
836 55. Wick RR, Judd LM, Gorrie CL, Holt KE. 2017. Unicycler: Resolving bacterial
837 genome assemblies from short and long sequencing reads. PLOS Computational
838 Biology 13:e1005595.
839 56. Seemann T. 2014. Prokka: rapid prokaryotic genome annotation. Bioinformatics
840 30:2068–2069.
841 57. Hamidian M, Ambrose SJ, Hall RM. 2016. A large conjugative Acinetobacter
842 baumannii plasmid carrying the sul2 sulphonamide and strAB streptomycin resistance
843 genes. Plasmid 87–88:43–50.
844 58. Gallagher LA, Ramage E, Weiss EJ, Radey M, Hayden HS, Held KG, Huse HK,
845 Zurawski DV, Brittnacher MJ, Manoil C. 2015. Resources for Genetic and Genomic

846 Analysis of Emerging Pathogen Acinetobacter baumannii. Journal of Bacteriology
847 197:2027–2035.
848 59. Arndt D, Grant JR, Marcu A, Sajed T, Pon A, Liang Y, Wishart DS. 2016.
849 PHASTER: a better, faster version of the PHAST phage search tool. Nucleic Acids Res
850 44:W16–W21.
851 60. Zankari E, Hasman H, Cosentino S, Vestergaard M, Rasmussen S, Lund O,
852 Aarestrup FM, Larsen MV. 2012. Identification of acquired antimicrobial resistance
853 genes. J Antimicrob Chemother 67:2640–2644.
854 61. Siguier P, Perochon J, Lestrade L, Mahillon J, Chandler M. 2006. ISfinder: the
855 reference centre for bacterial insertion sequences. Nucleic Acids Res 34:D32-36.
856 62. Derelle R, Wachsmann J von, Mäklin T, Hellewell J, Russell T, Lalvani A,
857 Chindelevitch L, Croucher NJ, Harris SR, Lees JA. 2024. Seamless, rapid and
858 accurate analyses of outbreak genomic data using Split K-mer Analysis (SKA). bioRxiv
859 https://doi.org/10.1101/2024.03.25.586631.
860 63. Stamatakis A. 2014. RAxML version 8: a tool for phylogenetic analysis and post-
861 analysis of large phylogenies. Bioinformatics 30:1312–1313.
862 64. Letunic I, Bork P. 2024. Interactive Tree of Life (iTOL) v6: recent updates to the
863 phylogenetic tree display and annotation tool. Nucleic Acids Research gkae268.
864 65. Yu G. 2020. Using ggtree to Visualize Data on Tree-Like Structures. Curr Protoc
865 Bioinformatics 69:e96.
866 66. Seemann T. 2015. snippy: fast bacterial variant calling from NGS reads.
867 67. Darling ACE, Mau B, Blattner FR, Perna NT. 2004. Mauve: Multiple Alignment
868 of Conserved Genomic Sequence With Rearrangements. Genome Res 14:1394–
869 1403.
870 68. Brown D, Cantón R, Dubreuil L, Gatermann S, Giske C, MacGowan A,
871 Martínez-Martínez L, Mouton J, Skov R, Steinbakk M, Walton C, Heuer O, Struelens
872 MJ, Högberg LD, Kahlmeter G. 2015. Widespread implementation of EUCAST
873 breakpoints for antibacterial susceptibility testing in Europe. Eurosurveillance
874 20:21008.
875 69. Tomaras AP, Dorsey CW, Edelmann RE, Actis LAY 2003. Attachment to and
876 biofilm formation on abiotic surfaces by Acinetobacter baumannii: involvement of a
877 novel chaperone-usher pili assembly system. Microbiology 149:3473–3484.

878 70. Ramirez MS, Don M, Merkier AK, Bistué AJS, Zorreguieta A, Centrón D,
879 Tolmasky ME. 2010. Naturally competent Acinetobacter baumannii clinical isolate as
880 a convenient model for genetic studies. J Clin Microbiol 48:1488–1490.
881 71. Niu C, Clemmer KM, Bonomo RA, Rather PN. 2008. Isolation and
882 characterization of an autoinducer synthase from Acinetobacter baumannii. J Bacteriol
883 190:3386–3392.
884 72. Jacobs AC, Thompson MG, Black CC, Kessler JL, Clark LP, McQueary CN,
885 Gancz HY, Corey BW, Moon JK, Si Y, Owen MT, Hallock JD, Kwak YI, Summers A, Li
886 CZ, Rasko DA, Penwell WF, Honnold CL, Wise MC, Waterman PE, Lesho EP, Stewart
887 RL, Actis LA, Palys TJ, Craft DW, Zurawski DV. 2014. AB5075, a Highly Virulent Isolate
888 of Acinetobacter baumannii, as a Model Strain for the Evaluation of Pathogenesis and
889 Antimicrobial Treatments. mBio 5:e01076-01014.
890 73. Antunes LCS, Imperi F, Carattoli A, Visca P. 2011. Deciphering the multifactorial
891 nature of Acinetobacter baumannii pathogenicity. PLoS One 6:e22674.
892 74. Godeux A-S, Lupo A, Haenni M, Guette-Marquet S, Wilharm G, Laaberki M-H,
893 Charpentier X. 2018. Fluorescence-Based Detection of Natural Transformation in
894 Drug-Resistant Acinetobacter baumannii. J Bacteriol 200:e00181-18.
895
896
897
898
899